Optical Pulling, Optical Deflection, and Optical Trapping of Single Airborne Particles using Negative Photophoresis

by

Adam Hart

April, 2016

Director of Thesis: Yong-qing Li

Major Department: Physics

Optical manipulation is the use of light to control the motion of objects. This thesis focuses on the development of optical transportation technology via optical pulling with application to the characterization of single airborne particles. Optical pulling, optical deflection, and optical trapping of single airborne particles using negative photophoresis force were demonstrated for the first time. Optical pulling and deflection were demonstrated for multiple absorbing particles. Raman scattering spectra of optically pulled particles were collected, thus demonstrating a method for particle identification. Using photography, digital video images were collected and analyzed for optically pulled and deflected particles. Optically pulled particles moved at a constant velocity for a given laser beam power. The velocity of optically pulled particles increased nonlinearly as laser power increased, approaching a saturation limitation. This saturation limitation was found to change with the atmospheric pressure. The efficiency for optical deflection was found to increase as the beam power ratio, deflection to pulling, increased approaching the limit of 100%. Using a fast photodiode, scattering light signals were collected from optically pulled and deflected particles, which were found to be periodic, suggesting a constant rotational frequency in the motion. This rotational frequency was found to depend on laser beam power. From the video images and scattering light data, theoretical models for optical pulling and optical deflection were derived. Optical manipulation and characterization of single airborne particles is of significance for the analysis related to air pollution, human health, and global climate change.

Optical Pulling, Optical Deflection, and Optical Trapping of Single Airborne Particles using Negative Photophoresis

A Thesis Presented To the Faculty of the Department of Physics

East Carolina University

In Partial Fulfillment of the Requirements for the Degree

Masters of Science in Physics

by

Adam Hart

April, 2016

OPTICAL PULLING, OPTICAL DEFLECTION, AND OPTICAL TRAPPING OF SINGLE AIRBORNE PARTICLES USING NEGATIVE PHOTOPHORESIS

by

Adam Hart

APPROVED BY:

DIRECTOR OF THESIS: _____

Yong-qing Li, Ph.D

Professor of Physics

COMMITTEE MEMBER: _____

Michael Dingfelder, Ph.D

Professor of Physics

COMMITTEE MEMBER: _____

Yu Yang, Ph.D

Professor of Chemistry

COMMITTEE MEMBER: _____

Jefferson Shinpaugh, Ph.D

Professor of Physics

DEAN OF THE GRADUATE SCHOOL: _____

Paul Gemperline, Ph.D

Professor of Chemistry

ACKNOWLEDGEMENTS

I would like to extend many thanks to Dr. Yong-Qing Li. First, I thank him for providing me with thesis direction as well as the facility, equipment, and funding to conduct this research. Secondly, I commend his patience with my student habits while at the same time fostering my educational growth through both the experimental and writing process. The knowledge and experience I gained from this research opportunity is invaluable and for this I am grateful. I would like to thank Dr. Micheal Dingfelder, Dr. Jefferson Shinpaugh, and Dr. Yu Yang for taking the time to serve on my thesis committee. I thank Dr. Jinda Lin for the additional guidance and knowledge inside the laboratory. I thank Dr. Shi-wei Wang and Josh Mangum for assistance during the data collection process.

I would like to thank the physics graduate department for providing me the opportunity to be part of the graduate program at ECU in pursuit of my academic interests. I would like to thank my parents for their continued love and support, especially financially, throughout these years of study.

Contents

List of Tables

List of Figures

1 Introduction

Optical manipulation is the use of light to control the motion of objects and sounds much like an idea from science fiction. In 1970, pioneer work by Arthur Ashkin was of the first to experimentally realize optical manipulation for various microparticles.[1] With the development of laser technology in the last 50 years,[2] there has been considerable attention to researching optical manipulation. Due to the variety of optical manipulation experiments, classification is necessary. This can be done by organizing experiments based on resulting particle motion and optical forces as shown in figure 1.

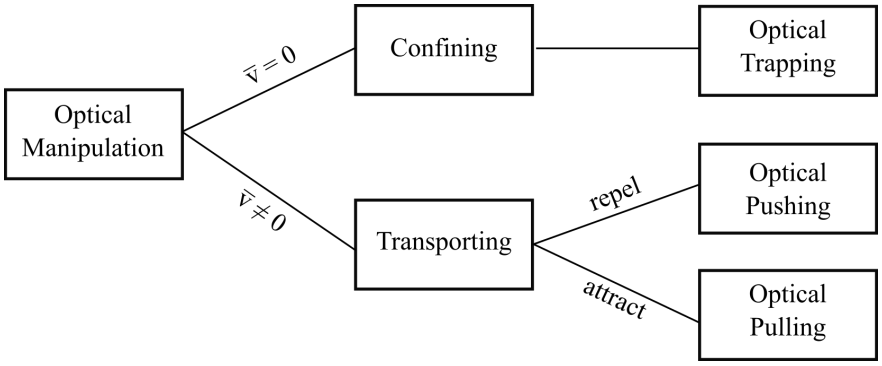

Figure 1: Optical Manipulation Classification

The particle motion may either be confining (zero average velocity, $\bar{v} = 0$) or transporting (nonzero average velocity, $\bar{v} \neq 0$). The optical forces may either be attractive or repulsive (a full treatment of optical forces will come later in this section). Experiments dealing with the optical confinement of particles are notably called "optical trapping" and may utilize either attractive or repulsive forces to trap particles. Experiments dealing with the optical transportation of particles depend on the resulting optical forces, with repulsion from the light source called "optical pushing" and attraction toward the light source called "optical pulling."

There is an increasing need to characterize bioaerosols and particulate matter in the air. Optical manipulation and characterization of single airborne particles is of significance for the analysis related to air pollution, human health, and global climate change. Optical trapping has been very

well demonstrated for particles in air and proves to be a useful tool in particle analysis, however, they are limited by the short range of their trapping regions. To overcome this limitation, an optical trap could be combined with an optical transportation system to effectively place the particle within the trapping region. Optical pulling could provide the transportation of particles to collection plates or optical traps, but optical pulling in air has not been realized. Optical pushing has been demonstrated over meter-scale distances in air,[3] however, this method faces many challenges for the collection of particles for long ranges. This thesis focuses on the development of optical transportation technology via optical pulling with application to the characterization of single airborne particles. This section explains the optical forces involved with optical manipulation, provides a brief history of optical manipulation development, and reveals the scope of study of this thesis.

1.1 Optical Forces

Because optical manipulation experiments are typically classified by the optical force they exploit, for example "optical levitation by radiation pressure," it is necessary to have some understanding of the optical forces involved before reviewing the field. This section provides an explanation of those optical forces.

One of the properties of light is that it can be treated as a particle, called a photon. Each photon carries energy of $\hbar\omega$ and momentum of $\hbar$k, where $\hbar$ is reduced Planck's constant, ω is angular frequency, and k is angular wave number.[4] Absorption, reflection or refraction of photons in the medium cause momentum change and produce radiation forces. Radiation forces can be classified into two forces: scattering and gradient. Figure 2 provides an illustration of these radiation forces.

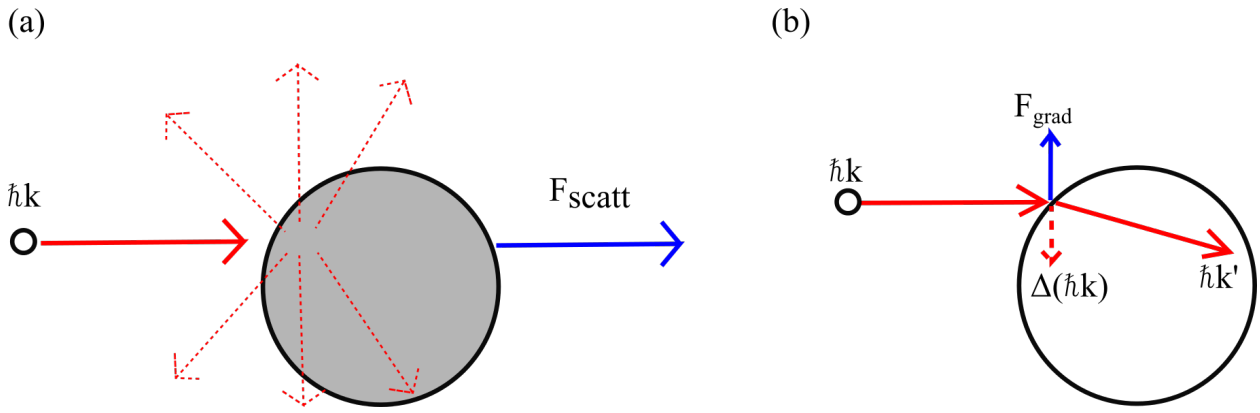

Figure 2: Forces of radiation pressure. (a) shows the scattering force (b) shows the gradient force.

The scattering force is due to reflection and absorption of light and is a direct transfer of the photon's momentum to the particle, much like a collision of two ordinary objects. The gradient force is the response to the change of momentum of the incident light due to refraction, light taking the path of least resistance when entering a different medium. For absorbing particles, the scattering force is significantly larger than the gradient force because most light energy is absorbed by the particle. For transparent and biological media, the gradient force is significantly larger than the scattering force as most light energy will transmit through in a bending direction.

When an object is illuminated, an increase in heat results from the energy transfer due to absorption. This increase in heat also causes the increase in temperature of a particle, making the particle hot. When suspended in a gas medium, the collisions of the surrounding gas with the illuminated "hot" object may induce motion, namely photophoresis.[5] There are two types of photophoresis forces: first type and second type. The first type of photophoresis force, $F_{\Delta T}$, is due to an inhomogeneous temperature of the illuminated particle. Figure 3 illustrates the first type photophoresis force. For particles with radius, a, larger than the wavelength of light, λ, the side of the particle immediate to the incident light has a higher temperature than the "shadowed side." This hot side transfers more momentum to the surrounding gas than the cold side resulting in a positive force, along the propagation axis of the light source. For particles with a radius much smaller than the wavelength of light, the hot side will be on the shadowed side, thus producing a negative force,

against the propagation axis of the light source. If the particles partially absorb light, the particle will serve as a spherical lens, focusing the illumination light to the shadowed side, making it hotter than the front side, thus producing a negative force as well.

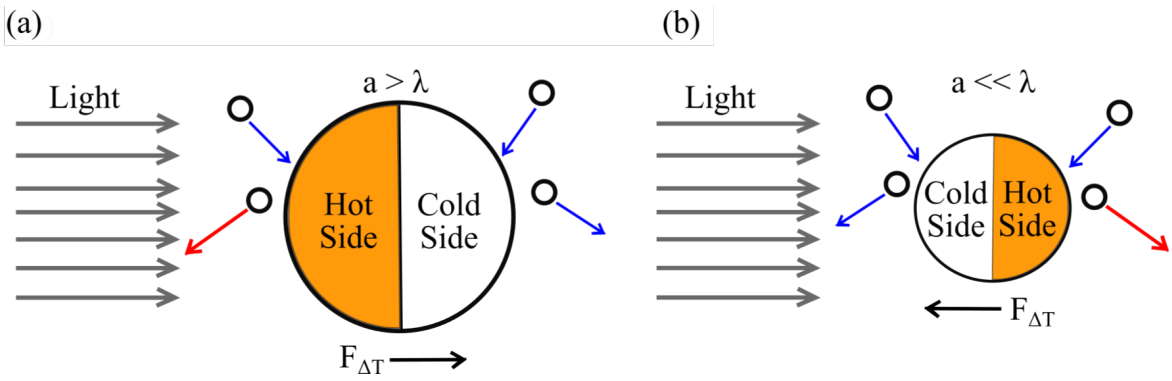

Figure 3: First type photophoresis force, $F_{\Delta T}$.(a) positive $F_{\Delta T}$ (b) negative $F_{\Delta T}$.

The second type of photophoresis force, $F_{\Delta\alpha}$, is due to a difference of accommodation coefficient, α, over the surface.[5] The accommodation coefficient is the ratio of the change in temperature of the gas molecule to the maximum allowable temperature exchange.[6] The accommodation coefficient depends strongly on the shape and surface properties of a particle. Even if the particle is heated evenly, as long as a particle has a temperature, T_w, different from the surrounding air and a varying accommodation coefficient, there will still be a net momentum exchange between the gas and particle. Figure 4 illustrates the second type photophoresis force. The gas molecules with temperature, T_0, hit on the side of higher accommodation coefficient and leave the surface faster with higher temperature, T, than the molecules hitting on the side of lower accommodation coefficient. This leads to a body-fixed force on the particle, pointing from the side of higher to the side of lower accommodation coefficient. The second type of photophoresis force may exhibit photophoresis in any direction.

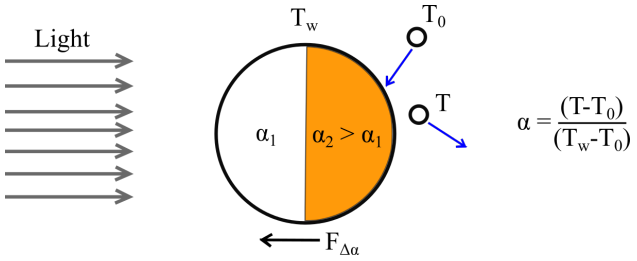

Figure 4: Second type photophoresis force, $F_{\Delta\alpha}$.

1.2 Brief History of Optical Manipulation Development

As mentioned earlier, this work is concerned with the development of optical transportation technology via optical pulling with application to the characterization of single airborne particles. While the complete history of optical manipulation is definitely interesting, it is beyond necessary to cover everything to understand the scope of this work. The methods and techniques of optical manipulation are numerous with a variety of applications extending across the natural sciences. To simplify the matter, I have selected the experimental development related to my categorization of optical manipulation by particle motion and the exploited optical forces (refer to figure 1). Figure 5 provides a brief history of optical of this development as well as a few notable applications.

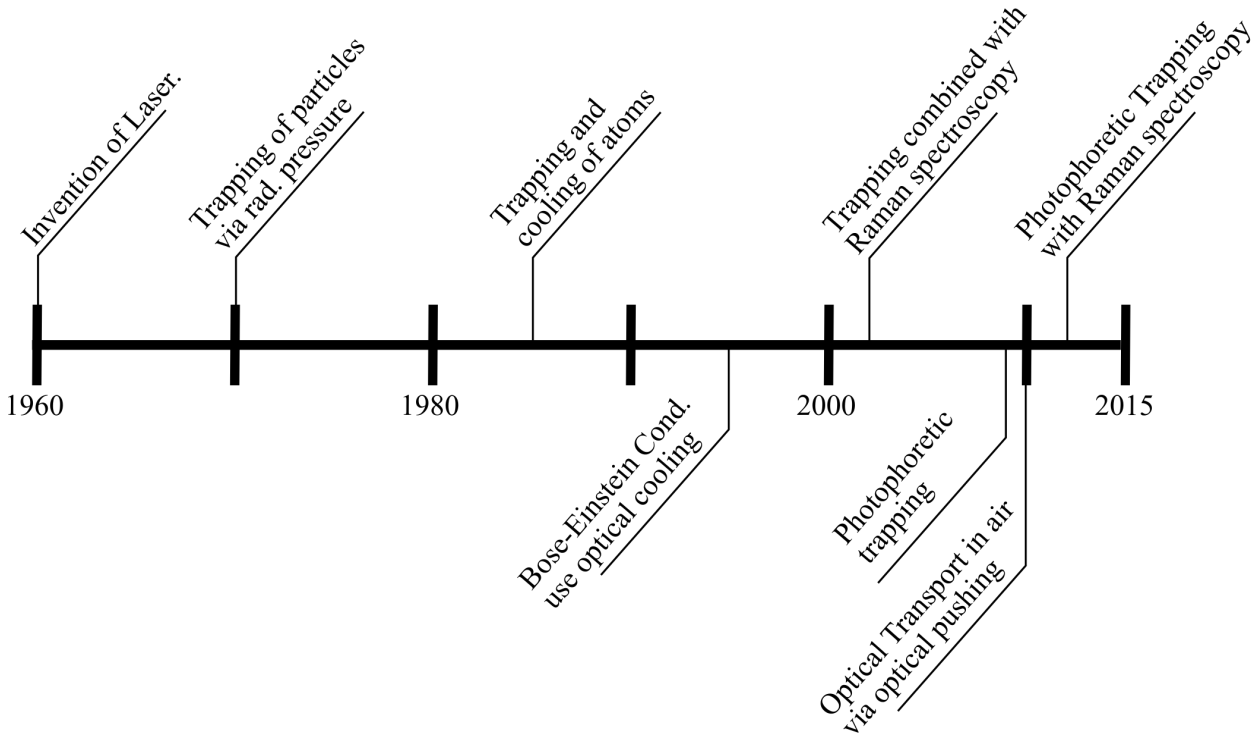

Figure 5: Brief history of optical manipulation

The invention of the laser in 1960 has single-handedly made the investigation of optical manipulation possible.[2] In 1970, Ashkin was the first to demonstrate optical trapping in liquid and air for various microparticles using radiation pressure.[1] This work serves as the foundation for the entire field. Two crowning achievements from optical trapping were the development of optical cooling technology in 1985 and the realization of Bose-Einstein condensation in 1995.[7,8] Nobel prizes were later awarded in 1997 and 2001, respectively, to those responsible for optical cooling and Bose-Einstein condensation. In 2002, Raman spectroscopy is combined with optical trapping for the purpose of particle "fingerprinting."[9] Raman spectroscopy is the detection of the inelastic scattering (energy loss) of light through a medium.[10] In 2009, photophoretic trapping is demonstrated for absorbing particles.[11] In 2010, optical transportation of particles in air is demonstrated on meter-scale distances using positive photophoresis, optical pushing.[3]

What has yet to be demonstrated is the optical transportation using negative photophoresis, optical pulling. It has been decades ago reported that irregular dusts under starlight illumination

are lifted in atmosphere against gravity and undergo helicoidally motion around the illumination direction.[12] Recently, it has been reported that light-absorbing particles can be optically trapped in air with a single focused Gaussian beam[13,14] and rotate around the laser propagation direction due to the negative photophoretic force.[15] Raman spectra of the trapped aerosols were measured to characterize the absorbing particles.[13,16] If atmospheric particles can be attracted by lasers over a long distance, they can be remotely collected for rapid identification.

1.3 Scope of Study

This thesis focuses on the development of optical transportation technology via optical pulling with application to the characterization of single airborne particles. These experiments are designed with the following questions of interest in mind:

1. Can negative photophoresis be the driving force of optical manipulation?
2. How can this be used to characterize single airborne particles?
3. What can be learned about light-particle interactions?

The optical pulling experiment is the backbone of this work with optical deflection and optical trapping as corollary experiments extending the application of optical pulling. This section provides the justification for these experiments.

1.3.1 Optical Pulling

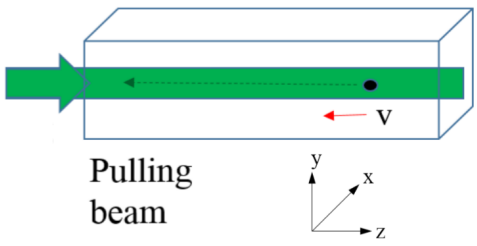

Figure 6: Schematic of optical pulling

Optical pulling is the attraction of objects back to the light source by the use of optically induced "negative forces," illustrated by figure 6. It is commonly expected that when illuminated by a collimated laser or gradientless light beam, an object will be accelerated along the light propagation direction by radiation pressure.[1] The idea of using optical beam to attract objects back to the light source is counterintuitive and has long been attractive to scientists.[17] Recent studies have proposed that small objects can be pulled against the light stream by a variety of mechanisms.[17–20] Optical pulling can be achieved using optical gradient force or optical tractor beams that attracts the object to the locations with higher light intensity.[20–22] Optical pulling could also be achieved by optical scattering force if the object can scatter incident light in a way that the forward momentum of the incident beam is less than that of the emergent beam.[18,23,24] The transportation of transparent particles with optical gradient force or optical conveyer was successfully demonstrated in a short range from a few to 10s micrometers in liquid media.[20,22] However, backward transportation of light-absorbing particles in air with laser beams has not been observed yet and it is usually considered that the absorbing particles are expelled by the scattering force and positive photophoretic force.[17] Here, we demonstrate that micron-sized absorbing objects can be optically pulled and manipulated over a meter-scale distance in air with a collimated laser beam based on negative photophoretic force.

When micron-sized objects are suspended in air and illuminated by a laser beam, strong photophoretic forces can be induced due to the heating by light,[5,25,26] which can be several orders of magnitude larger than the radiation force and gravitation force.[3] For high-absorbing microparticles, there is more absorption on the illuminated side and, therefore, a positive photophoretic force $F_{\Delta T}$ is usually induced,[5] pushing the absorbing particles away from the high intensity region of a laser beam. Optical pulling of high-absorbing particles is not allowed by the first type of photophoretic force $F_{\Delta T}$. However, the second type of photophoretic force $F_{\Delta\alpha}$ can be negative,[5,26] allowing the particle to move back to the light source. It remains unclear to what degree $F_{\Delta\alpha}$ and $F_{\Delta T}$ might contribute, but they can coexist for irregular particles. It was estimated that under atmospheric pressure or below, practically $F_{\Delta\alpha}$ force is dominant for micron-sized particles.[5,25,26]

1.3.2 Optical Deflection

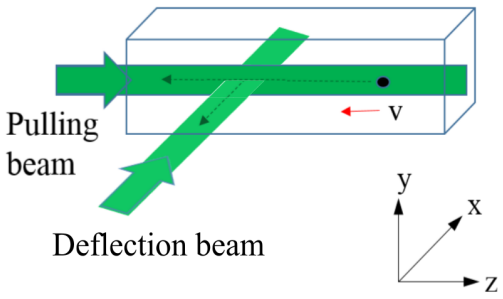

Figure 7: Schematic of optical deflection

Optical deflection is the change in the direction of motion due to the action of another light source, illustrated by figure 7. Optical deflection has not been previously demonstrated, however, if optical pulling can be achieved with a collimated light source, then the demonstration of optical deflection should be observed when another light source of the same type intersects the original source. Here, we demonstrate that micron-sized absorbing objects can be optically deflected over a meter-scale distance in air with collimated laser beams based on negative photophoretic force.

1.3.3 Optical Trapping

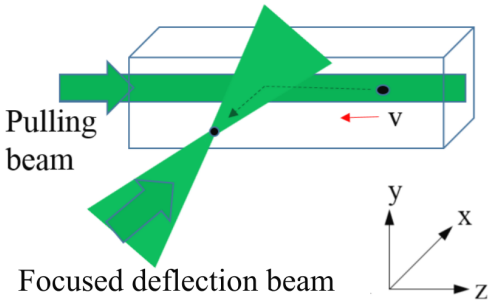

Figure 8: Schematic of optical trapping

Optical trapping is the confinement of a particle motion with optically induced forces. As stated earlier, optical trapping is a useful tool for particle analysis. Optical trapping using negative photophoresis force has been previously demonstrated and on top of that been demonstrated using Raman spectroscopy for single particle identification.[13,15] Here, we demonstrate that micron-sized absorbing objects pulled along an optical pipeline can be optically deflected and trapped with a focused laser beam based on negative photophoretic force, illustrated by figure 8.

2 Experimental Setups and Operating Procedures

This section provides the experimental setups for optical pulling, optical deflection, and optical trapping. There are many shared components across the three setups. Unless explicitly discussed, the details of experimental components are found in Appendix A.

2.1 Optical Pulling

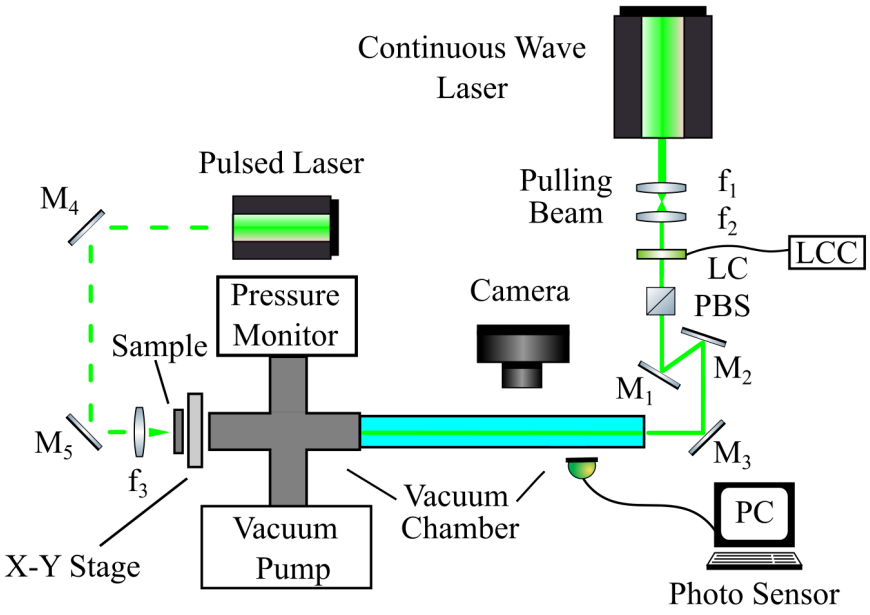

Figure 9: Experimental Setup for Optical Pulling.

The experimental setup for optical pulling is shown in figure 9. The continuous-wave laser provides a collimated Gaussian beam at a wavelength of 532 nm. The combination of focusing lenses with focal lengths, f_1 and f_2, reduce the incident beam diameter, d_0, as shown in figure 10.

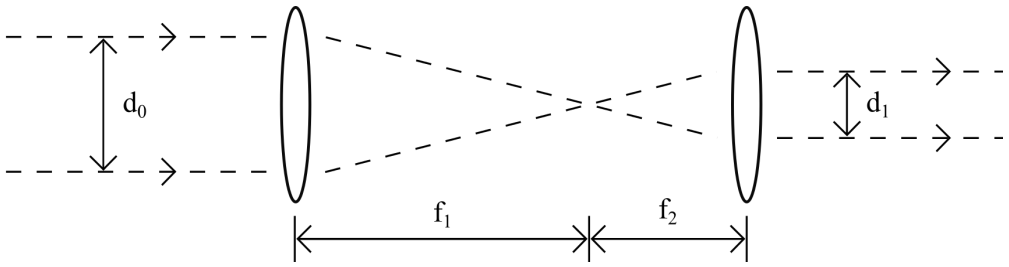

Figure 10: Beam reduction diagram.

The emerging beam diameter, d_1, is determined by the equation

$$d_1 = d_0\left(\frac{f_2}{f_1}\right)$$

The liquid crystal (LC) functions as a variable half-wave plate through the control of the liquid crystal controller (LCC). The polarizing beam splitter (PBS) splits the laser beam depending on the laser's polarization state, illustrated by figure 11. The perpendicularly polarized beam was blocked as it was not used in the experiments. The LC and PBS provide selective power control independent of the laser beam's power supply.

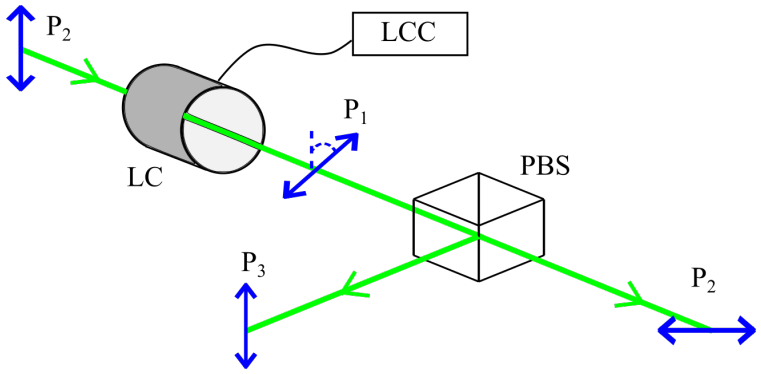

Figure 11: Power control through LC and PBS with polarization shown in blue. The linearly polarized beam with power P_1 passes through the LC only changing polarization state. The beam then passes through the PBS and is split into two beams, one with parallel polarization and one with perpendicular polarization. These beams have power P_2 and P_3 where $P_2 + P_3 = P_1$.

Highly reflective mirrors, M_1, M_2 and M_3, provide the alignment for the laser beam to the entrance window of the vacuum chamber. Figure 12 shows an actual picture of the vacuum chamber and connected parts.

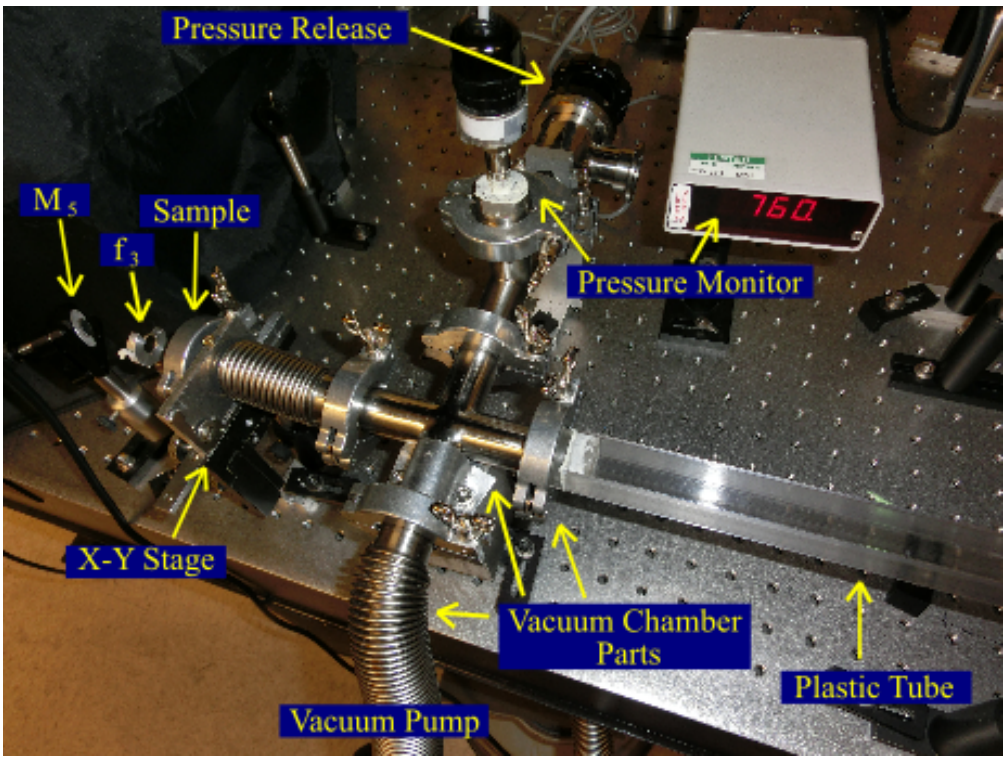

Figure 12: Vacuum Chamber Picture. The vacuum pump is tucked under the optics bench. Only a portion of the plastic tube is pictured.

The pulsed laser provides a method of ablation for the sample. The mirrors M_1 and M_5 align the pulsed laser "pulses" coincident with the continuous-wave laser beam. A focusing lens with focal length f_3 focuses the laser pulses to ablate a small area of the sample. The X-Y stage provides a method of moving the sample.

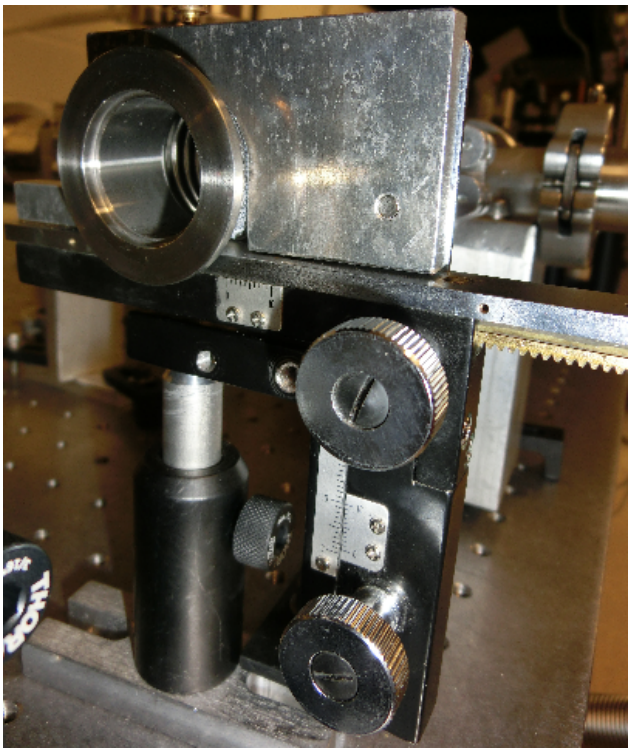

Figure 13: Image of custom X-Y stage. It is made by modifying a mechanical micrometer with a custom made metal piece to fit around the $4''$ metal hose. The custom X-Y stage takes advantage of the flexibility of the metal hose.

The camera records video observations. The photo sensor records the scattering light signal from the transported particle.

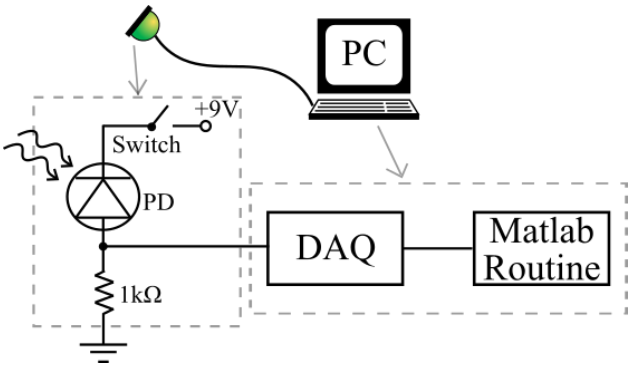

Figure 14: Diagram of the photo sensor. The photo diode is reversed biased. The signal is received by a data acquisition card (DAQ), which converts the signal from analog to digital. The digital signal is then processed by a software routine written in Matlab, a computational software. The Matlab interface can be found in Appendix B.

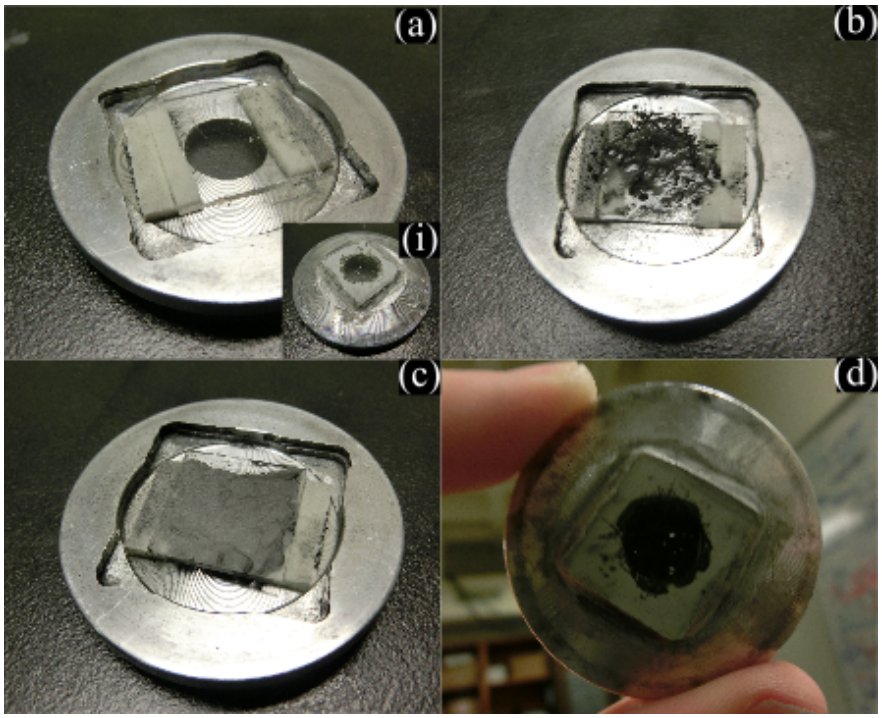

Figure 15: Sample preparation. (a) The sample holder is a modified NW25 blank flange with hole bored through the middle. The sample glass is attached to double-sided foam tape. This isolates the outside glass seen in (i) from potential damage from the focusing of the pulsed laser. (b) A small layer of alcohol is placed on the surface of the glass before the sample is placed. This allows the sample to adhere to the surface when under vacuum conditions as well as smoothing of the sample. (c) The sample after smoothing process using the air from a clean, empty pipette. (d) Sample thickness should be just thick enough to be opaque.

The sample is prepared as shown in figure 15. The sample is attached to the custom X-Y stage after the sample preparation. The pressure is reduced. The camera is mounted and positioned above the transparent portion of the vacuum chamber. The photo sensor is placed underneath the same portion. The pulling beam power is adjusted by the LCC depending on the sample and the application. Power measurements are made at the entrance window of the vacuum chamber and the voltage of the LCC is adjusted. The system at this point only requires input pulses from the pulsed laser onto the sample to achieve pulling. Once the pulses are fired, some time (around 10

sec maximum) was allowed for the pulled particles to show inside the visible portion. The position of the sample is adjusted such that pulling beam was aligned with the sample and the pulsed laser process repeated.

2.2 Optical Deflection

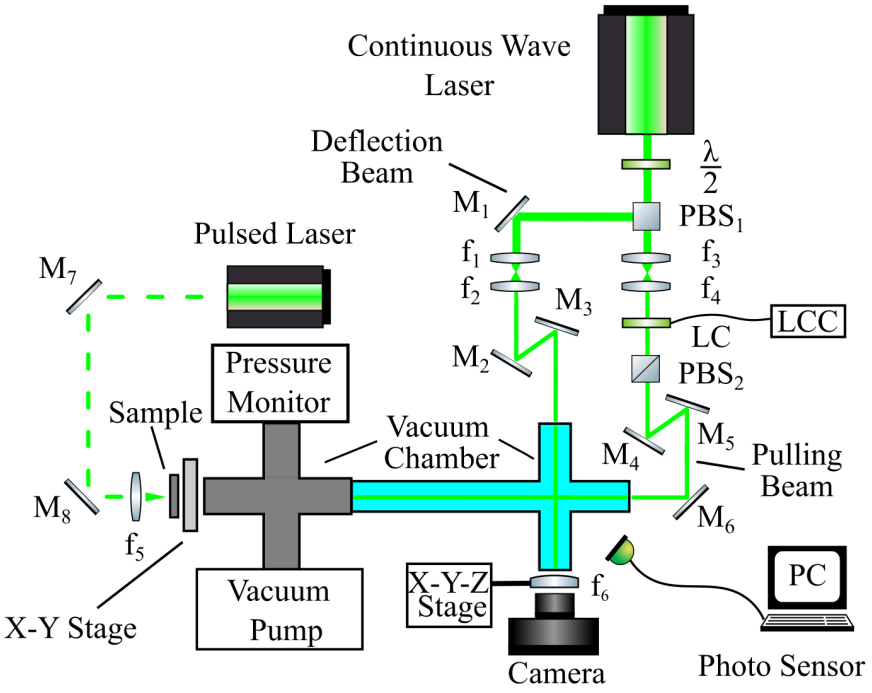

Figure 16: Experimental Setup for Optical Deflection.

The experimental setup for optical deflection is shown in figure 16. The setup is essentially the optical pulling scheme with the addition of an intersecting "deflection" beam. The half-wave plate, $\frac{\lambda}{2}$ combined with the PBS_1 provides a method of adjusting the beam splitting ratio. Focusing lenses f_1,f_2 reduce incident beam size. Objective lens, f_6, transforms the camera into a video microscope for high-speed data. The X-Y-Z stage allows adjustments of the objective lens' alignment position and focal plane. The sample is attached to the custom X-Y stage after the sample preparation. The LCC is set to allow full power transmission through PBS_2. The half-wave plate is adjusted such that the deflection beam and pulling beam have the power required at their respective entrance windows to the vacuum chamber. The pulling beam is calibrated through the LCC depending on sample and application. The camera is mounted above the transparent portion of the vacuum chamber.

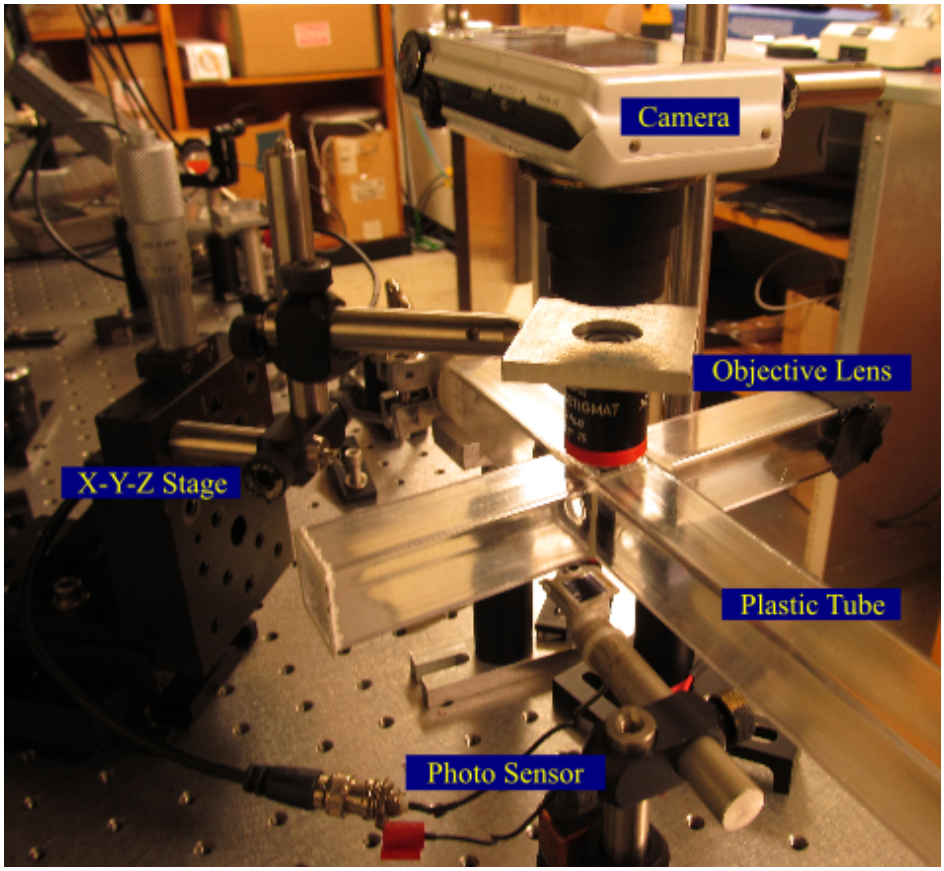

Figure 17: Image of High-speed Video Setup

For high-speed video imaging, camera position and objective alignment was aided with the use of Rhodamine B fluorescent dye solution as seen in figure 18.

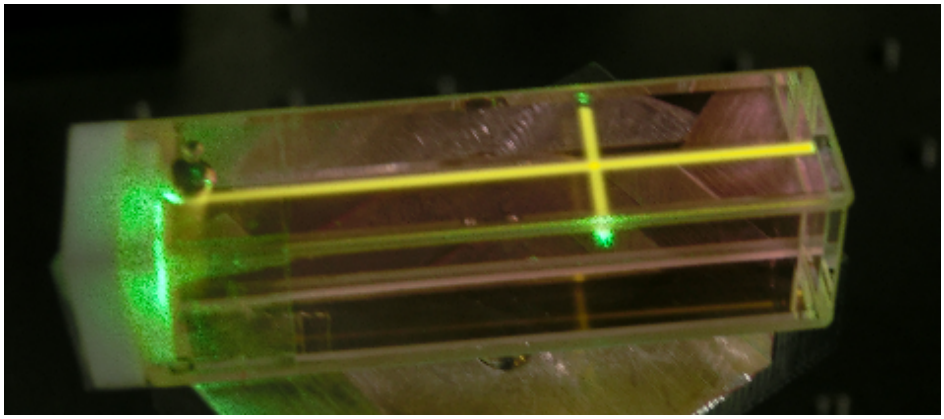

Figure 18: Image of Rhodamine B dye solution. The solution is diluted by distilled water to reduce the intensity of the fluorescence.

The transparent portion of the vacuum chamber is removed for this calibration. The objective's focal plane adjusted to the cross-section in the middle of the intersection region of the deflection and pulling beams. The transparent portion is reattached and pressure is reduced. The photo sensor is positioned below the intersection region. The input pulses are fired from the pulsed laser. Once the pulses are fired, some time (around 10 sec maximum) was allowed for the pulled particles to show inside the visible portion. The sample X-Y stage is adjusted such that pulling beam is aligned with the sample and the pulsed laser process repeated.

2.3 Optical Trapping

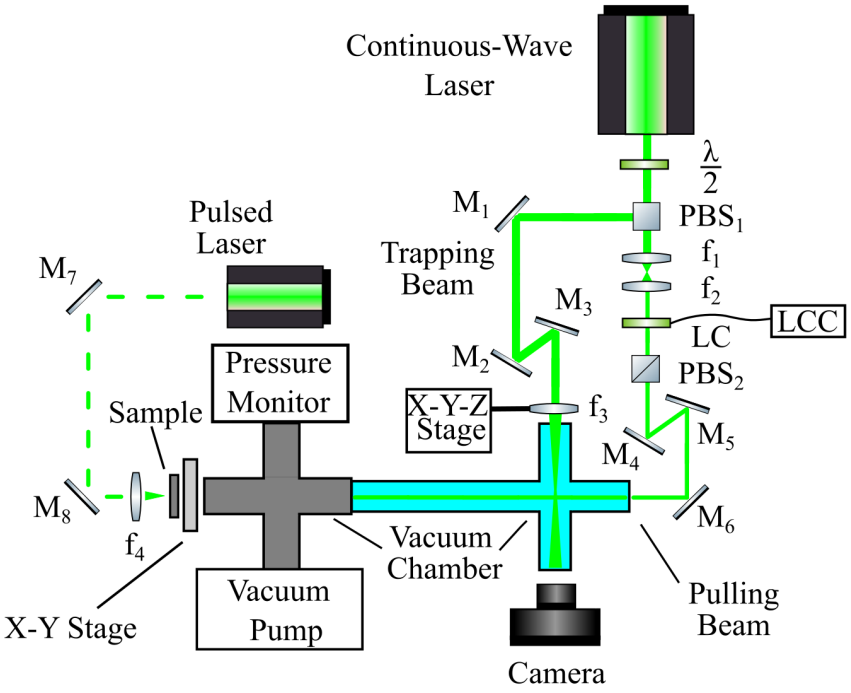

Figure 19: Experimental Setup for Optical Trapping.

The experimental setup for optical trapping is shown in figure 19. This is essentially the optical deflection scheme with the removal of beam reduction components and addition of a focusing lens. The focusing lens, f_3, provides the optical gradient required for a single-beam optical trap. The X-Y-Z stage allows the position of f_3 to be adjusted.

The sample is attached to the custom X-Y stage after the sample preparation. The LCC is set to allow full power transmission through PBS_2. The half-wave plate is adjusted such that the trapping beam and pulling beam have the power required at their respective entrance windows to the vacuum chamber. The pulling beam is calibrated through the LCC depending on sample and application. The pressure is reduced. The camera is mounted and positioned above the transparent portion of the vacuum chamber. The input pulses are fired from the pulsed laser. Once the pulses are fired, some time (around 10 sec maximum) was allowed for the pulled particles to show inside the visible portion. The sample X-Y stage is adjusted such that pulling beam is aligned with the

sample and the pulsed laser process repeated.

3 Results

3.1 Optical Pulling

Video demonstration of optical pulling can be found on the CD provided. The demonstration is of a few carbon particles pulled over a meter scale distance with a collimated laser beam at constant power. The laser beam was operated in TEM_{00} mode with linear polarization (y-direction) and beam diameter of $\sim$1 mm.

3.1.1 Translational Motion Under Constant Pulling Power

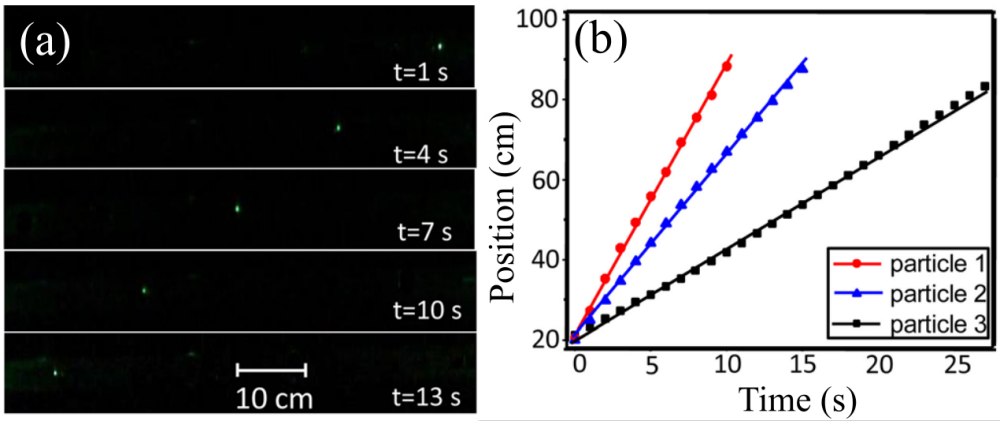

Figure 20: (a) Evolution of a pulled particle over 5 selected frames. (b) Position-time graph for three individual carbon particles pulled by a 150 mW pulling beam at 110 Torr.

The translational motion of the highly absorbing particles was analyzed when pulled by a constant beam power. From the time-lapse video images, the position of the carbon particle was tracked in a number of frames using Tracker, an open source software designed for motion analysis (version: 4.91). Figure 20.a shows the time evolution of carbon nano-cluster ($\sim 10\mu$m in size) as pulled through the vacuum chamber. The positions are obtained for a number of frames and plotted as shown in figure 20.b. The pulling speed of these particles were measured to be 6.8, 4.5, and 2.3 cm/s, respectively. It should be noted that the ejection of particles off the sample window is

due to the effect of laser induced forward transfer induced by the pulsed laser.[27] The motion of the particle against the continuous wave laser at a constant speed is the result of negative photophoresis force induced by the continuous wave beam. When the continuous wave laser is blocked, the translational velocity of the particle is quickly reduced by Stokes drag force and moves off the beam axis due to gravitation force.

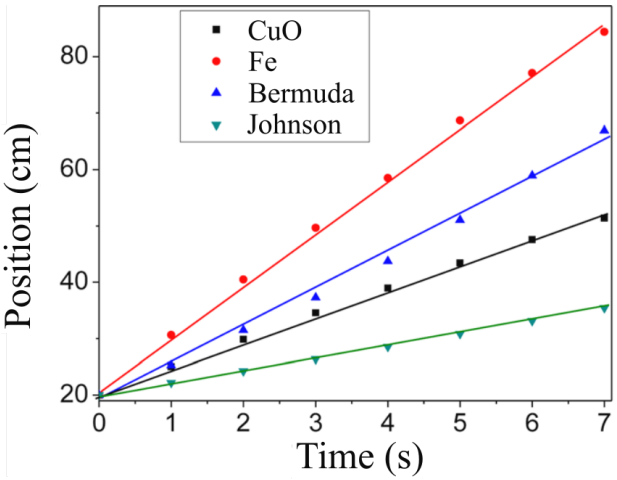

Figure 21: Position-time graph of four individual particles at 110 Torr that were pulled by a laser with a constant power of 150 mW for Bermuda grass smut spores, 200 mW for iron filings, and 300 mW for Johnson Grass smut spores and CuO power.

Optical pulling was performed for other absorbing particles. Figure 21 provides the plot of position versus time of these particles. It is clear from both of the position versus time plots that all positions of the absorbing particles increase linearly while being pulled by a constant power laser beam. Since the particles showed the same behavior in the position-time plots, it is reasonable to suspect that *all* highly absorbing particles exhibit the same motion with differences only due to particle properties.

3.1.2 Translational Motion Under Varied Pulling Power

The dependence of the translational speed of each individual particle on the laser intensity was measured. This was done by changing the power of the pulling laser every 1.5 s during the particles

motion through the LCC by an external voltage signal. Figure 22 displays the results of the data extracted from video observation for carbon nano-clusters. Figures 22.a-22.c show the changes in the pulling speed of five individual particles when the laser power was decreased from 150 to 30 mW at different gas pressures of 110, 30, and 8 Torr, respectively.

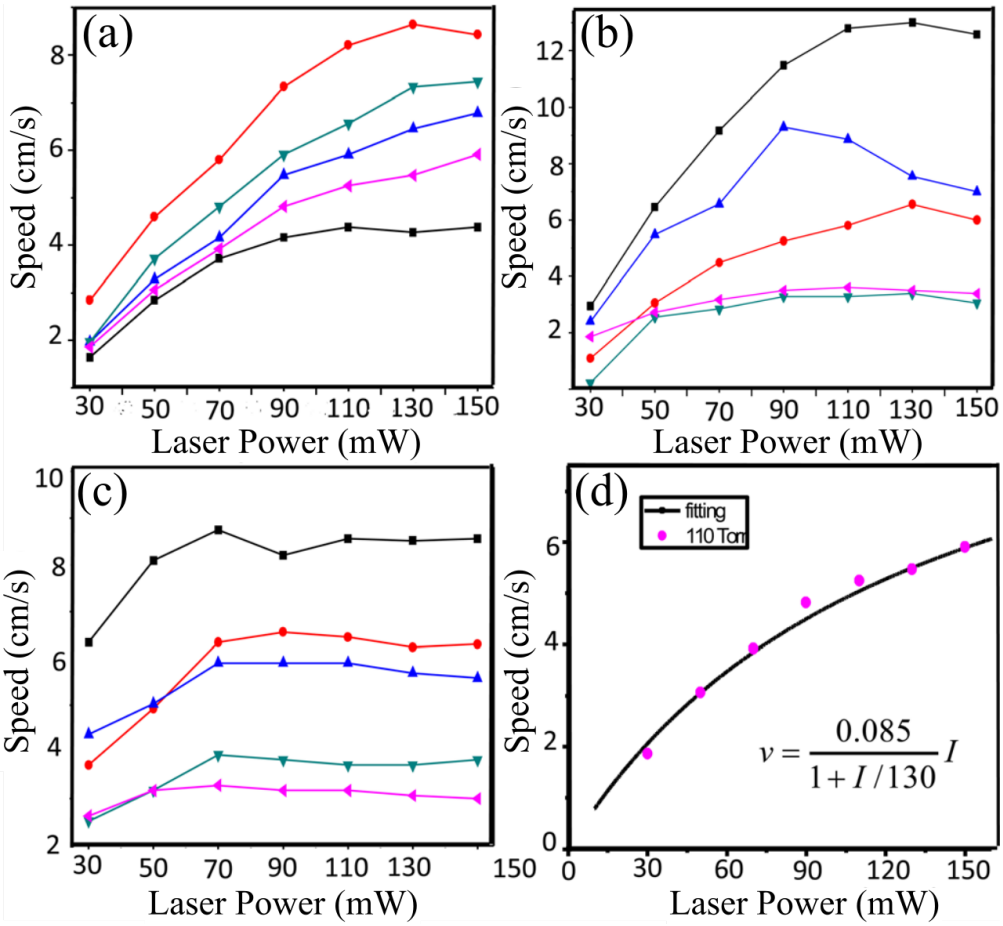

Figure 22: Speeds of five individual carbon particles with different laser powers at (a) 110 Torr; (b) 30 Torr; (c) 8 Torr. (d) The fitting of the pulling speed v of a particle at 110 Torr with different laser powers.

The results indicate that: (1) at a given pressure, when the laser power is decreased the pulling speed decreases; (2) as the laser power exceeds a saturation power, the pulling speed reaches a maximum value; and (3) as the gas pressure is decreased, the saturation laser power decreases. Accordingly, lower laser power is required to pull the absorbing particles with the same speed at

low pressure. However, the averaged maximum pulling speed over about ten individual particles was nearly the same at different pressures. The average saturation laser power was found to be 115±19, 83±31, and 78±14 mW for the pressure of 110, 30, and 8 Torr, respectively, while the average maximum speed was 6.0±2.1, 6.4±3.1, and 5.5±1.6 cm/s, respectively.

The translational speed of a pulled absorbing particle not only depends on particles properties (e.g., particle size and shape), but also depends on laser power and the pressure of the gas medium. For a given particle, when the gas pressure and laser power are changed, the speed of the particles motion changes accordingly.

3.1.3 Rotational Motion Under Constant Pulling Power

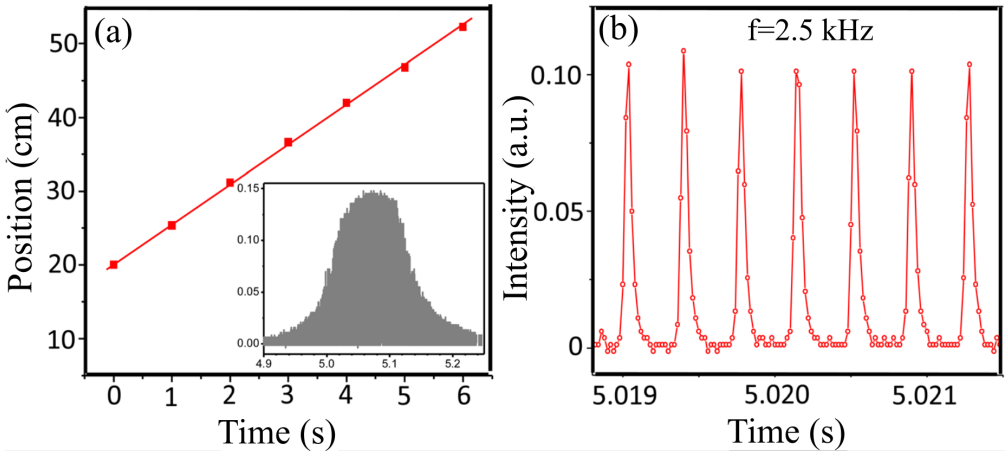

Figure 23: (a) Position-time graph of a carbon nano-cluster pulled at a speed of 5.4 cm/s with a constant power of 150 mW at 110 Torr. The inset is the profile of the scattered light signal as detected by the photodiode. (b) The intensity of the scattered light in a small time-scale changes periodically, indicating that the particle rotates with a frequency of 2.5 kHz.

The motion of absorbing particles in a optical pulling beam is conjectured to be a helical motion toward the laser source[5].[12] The particle undergoes a rotation motion at a high speed while moving toward the entrance window at a constant axial speed. To verify this, the scattered light of the pulling laser beam from the particle was measured using a photodiode.[15] When the particle was

pulled and passed through the detection region of the photodiode, the intensity of the scattered light from the particle in the perpendicular direction to the laser beam axis was collected, as shown by the inset of figure 23.a. The variation in the signal intensity, as seen in figure 23.b, suggests that the light scattering from the absorbing particle is highly directional due to particles rotation, which may direct the scattered light to a rotating direction. This idea is supported by similar study that measured the direct relation between the variation frequency in the scattered light intensity and particles rotation frequency with a high-speed imaging technique.[15] The particle shown in figure 23 was pulled with an axial speed of 5.4 cm/s while rotating around the beam axis at a frequency of 2.5 kHz. The rotation frequencies of different particles were found to varying from 0.2-10 kHz.

3.1.4 Imaging and Raman Scattering

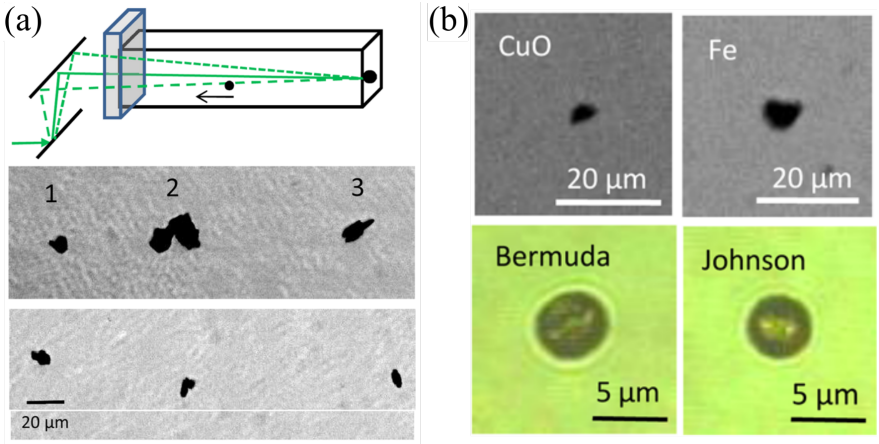

Figure 24: (a) Remote manipulation using optical pipeline. Individual particles can be manipulated in transverse direction and thus precisely positioned on different locations of the entrance glass window by steering the direction of the pulling laser beam. Insets are images of three carbon particles that were positioned in a row along the x direction. (b) Micrograph of other pulled particles.

Steering the propagation direction of the pulling laser beam allows the manipulation of the pulled particles in x-y directions and thus enables precise control of the location on which the particle adheres on the entrance glass window. As a result, individual particles can be positioned in one-dimension or two-dimension patterns, as shown in figure 24.a. After the particles were positioned on the entrance glass window, they were measured with a micro-Raman spectroscopy system equipped with an inverted microscope (IX81, Olympus), an excitation laser at 780 nm, an imaging spectrograph, and a multichannel CCD detector.[28] Insets in figure 24.a show the microscopic images of three individual carbon particles that were positioned in a row with a positioning accuracy of $\sim 20\mu$m over the distance of $\sim$1 m. The particles had sizes of 5-20 μm with irregular shapes. Figure 24.b shows the micrographs of the other absorbing particles.

Figure 25 shows the Raman spectra of three individual collected particles and the peaks at $\sim$1573 and $\sim$1310 cm^{-1} represent the G-band and D-band of carbon particles.[13,16] These results confirmed that the carbon particles were pulled from the sampling region near the back window to the entrance window over a meter along optical pulling pipeline.

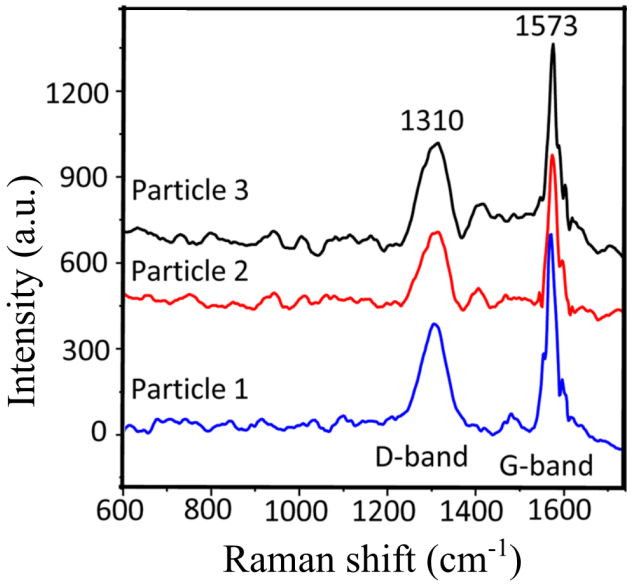

Figure 25: Micro-Raman spectra of the three collected individual carbon particles seen in figure 24. The laser intensity for the Raman excitation was 1 mW at 780 nm with an acquisition time of 50 s.

3.2 Optical Deflection

Video demonstration of optical deflection can be found on the CD provided. The demonstrations record the deflection for carbon nano-clusters, bermuda spores, and iron filings. The carbon nano-clusters were pulled at 75 mW with a 112 mW deflection beam. The bermuda spores were pulled at 150 mW with a 150 mW deflection beam. The iron filings pulled at 190 mW with a 190 mW deflection beam. The pressure was reduced to 110 Torr for all particles.

3.2.1 Deflection Efficiency

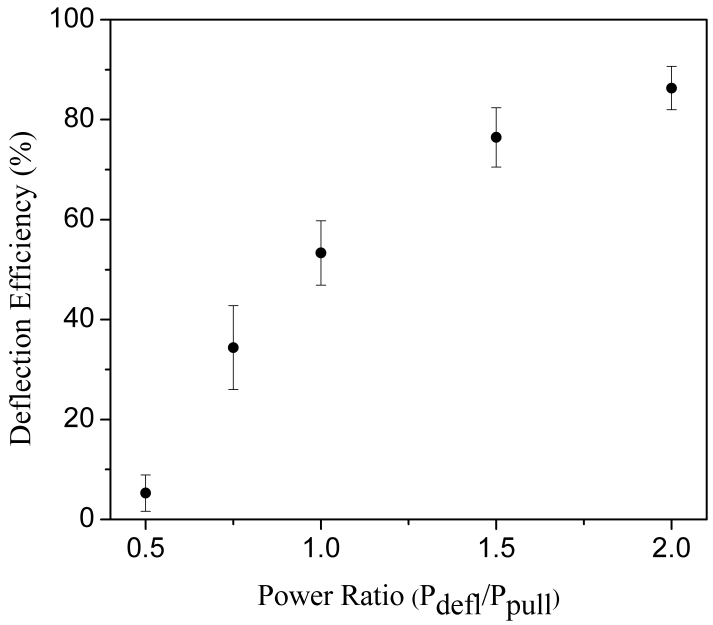

Figure 26: Deflection efficiency for carbon nanoclusters pulled at 75 mW at 110 Torr.

A graph of deflection efficiency for carbon nano-clusters pulled at 75 mW at 110 Torr is shown in figure 26. The deflection efficiency is the ratio of the amount of particles that deflect into the deflection beam from the pulling beam to the total amount of successfully pulled particles. A successfully pulled particle was one that traveled more than 95% of the total pulling distance (majority of the counted particles traveled 100%). Also, a successful deflection required the particle

Table 1: Deflection Efficiency Data for Carbon nano-clusters

Deflection Power (mW)	Power Ratio	Total Particles	Total Deflected	Percent (%)	Error (±)
32	0.5	38	2	5.26	3.62
56	0.75	32	11	34.3	8.40
75	1	60	32	53.3	6.44
112	1.5	51	39	76.5	5.93
150	2	73	63	86.3	4.33

to be deflected via negative photophoresis force (a very small percentage of particles may be optically "pushed" by the deflection beam after being intially pulled). The data seen in figure 26 was obtained by a series of video observations. The values from observation are provided in table 1. It is clear by figure 26 that the deflection efficiency increases when the power ratio increases, approaching the limit of 100%.

3.2.2 Position and Velocity Measurements

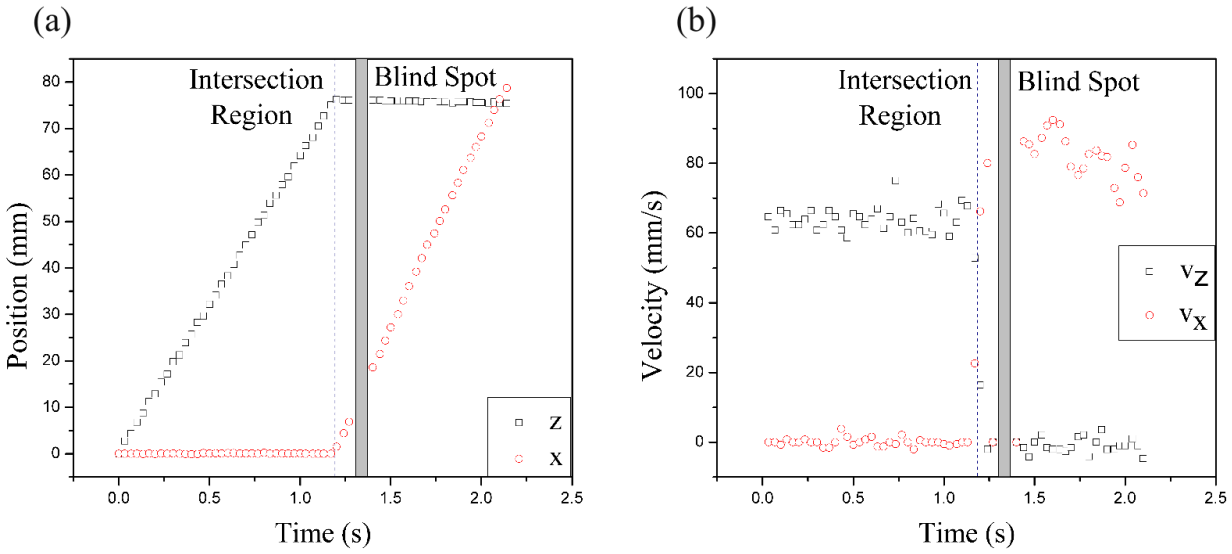

Figure 27: Deflection data of a carbon particle. The blind spot is due to a joint seal in the vacuum chamber tube.

The position and velocity data was obtained using Tracker (version: 4.91) for carbon nano-clusters. The carbon nano-clusters were pulled at 75 mW at 110 Torr with a 112 mW deflection beam.

Figure 27 shows the graphs of the position and velocity measurements for a single carbon particle. Figure 27.a shows a linear increase in position along both the pulling axis (z-direction) and, after deflection, the deflection axis (x-direction). Supporting the linearity, figure 27.b shows that the average velocity along pulling and deflection axes is constant.

3.2.3 High-Speed Video Data

High-speed video is found in the provided CD. The video was zoomed and focused to the closest distance that all regions - pulling, intersection and deflection - could still be discerned. The resolution of the image frame was determined to be 24 μm/pix. To give a sense of size, the scattering light from the first and third particle in the video measured 48 μm across as measured perpendicular to the particle motion. The video was recorded at 1000 fps with a 2.5 OD (optical density) neutral density filter in front of the camera. The image of the fluorescence was edited into the background to give a sense of location of the particles within the laser beam. There is some uncertainty to the actual location of the beams when compared to the fluorescent background image.

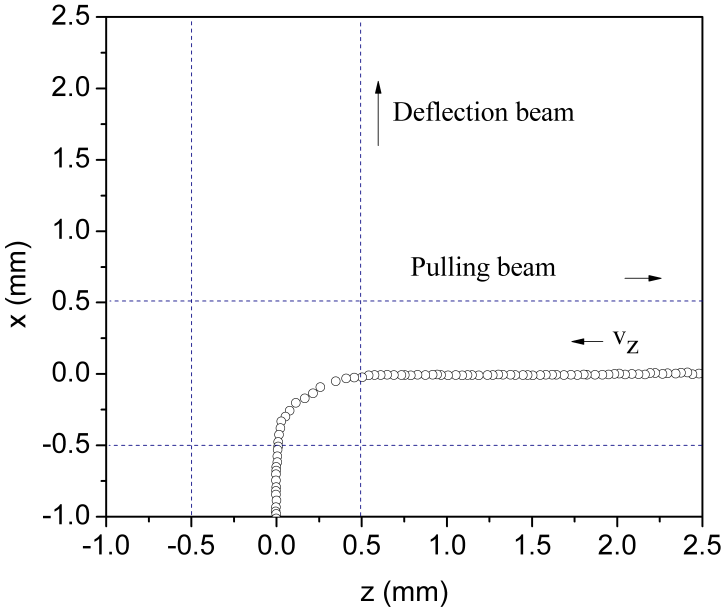

Figure 28: Plot of trajectory of a carbon nano-cluster particle with assumed beam location.

The position data of a deflected carbon nano-cluster was obtained from Tracker. Figure 28 shows the plot of its trajectory. While solely in the pulling or deflection beam, the particle tends to travel near the center of the beam. While in the intersection region, the particle follows a curved path during the deflection.

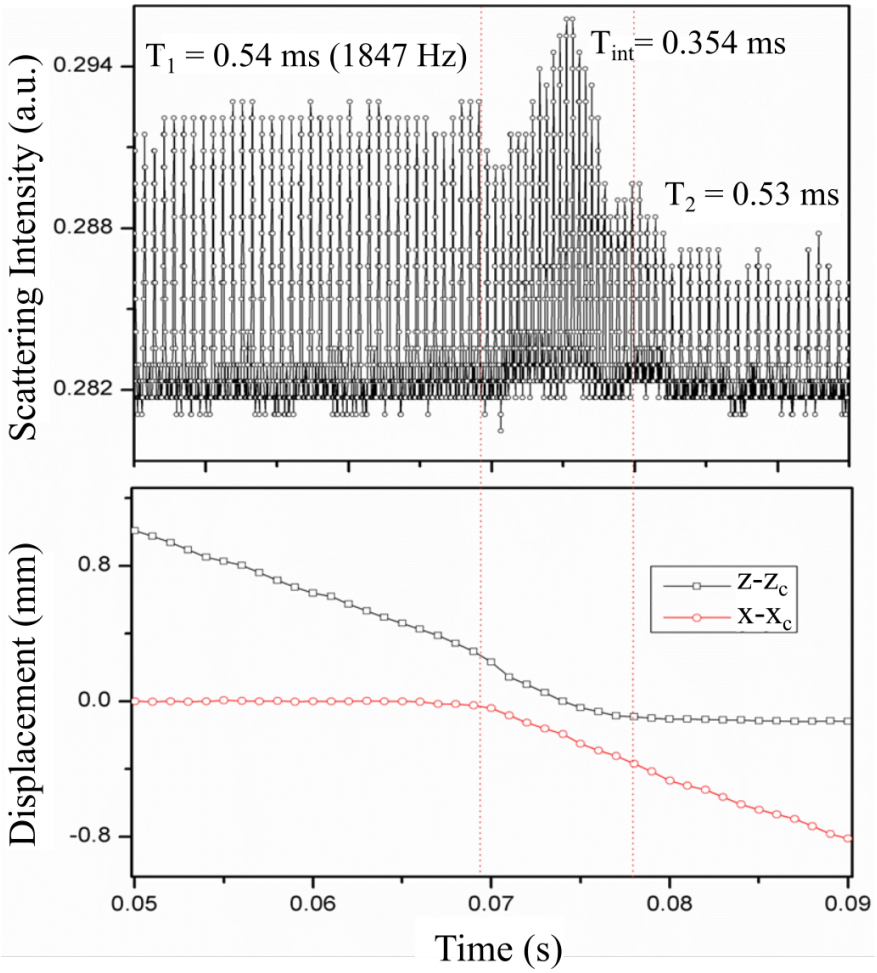

Figure 29: Scattering data combined with position data. z_c and x_c are the coordinates of the center of the intersection region.

The scattering light signal the for the same carbon nano-particle is plotted in figure 29. The signal shows three distinct frequencies which correspond with the three regions: pulling, intersection, and deflection. The particle traveling along the pulling beam has a rotational period of T_1. When the particle enters the intersection, the rotational period decreases to T_{int}. When leaves the

intersection into the deflection beam, the rotation period increases to a value T_2 comparable to T_1. As a confirmation of the previous described behavior, figure 29 maps the scattering light signal obtained from the photo sensor to the position data obtained from video observation.

3.3 Optical Trapping

A video demonstrating the successful capture of a single absorbing particle off an optical pulling beam is found on the provided CD. Video settings were standard video settings with manual focusing at 30 fps. The trapping beam was calibrated to have a power of 112 mW with a diameter that matches that of the pulling beam at the intersection. The particle is being pulled at 75 mW at 110 Torr. Figure 30 provides select frames from the video to illustrate the manipulation of the particle within the optical trap.

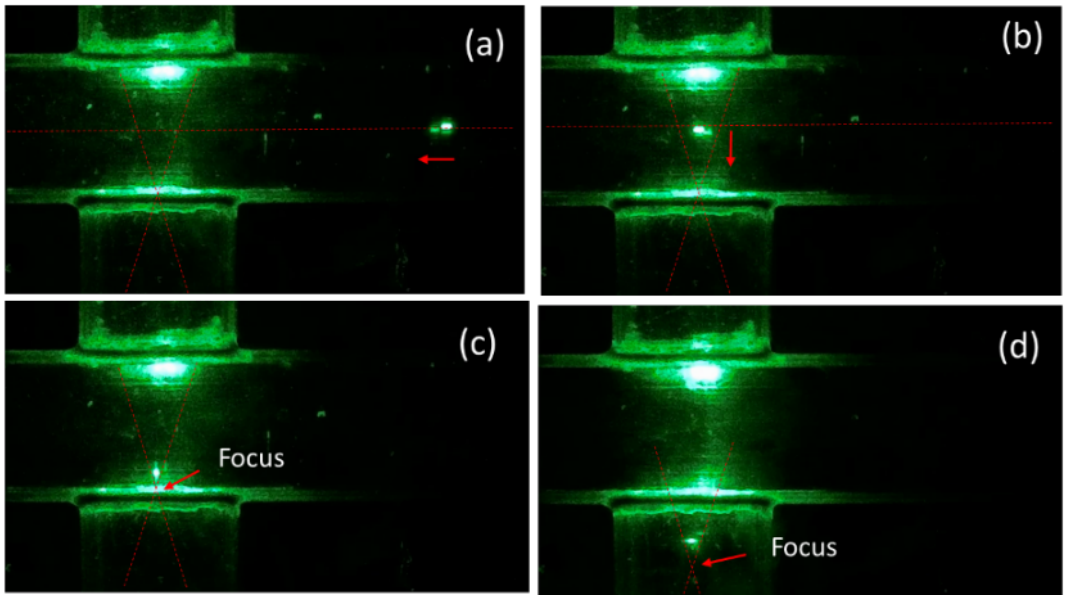

Figure 30: (a) Particle on approach in the pulling beam. (b) Particle arriving at the intersection of the pulling beam and trapping beam. (c) Particle takes to the optical trap and is trapped near the focus of the focusing lens. (d) The position of the focus was moved away from the pulling beam to further demonstrate that the particle is solely trapped. (Note: the focus diagram is just a visual aid and not scaled to actual beam size)

4 Discussion

4.1 Optical Pulling

From the motion data obtained, a theoretical model can be adapted to describe the situation. When a particle is pulled with a laser intensity I and moves with a constant speed v along negative z-direction (beam axis), the resultant force is balanced,

$$\sum \mathbf{F} = \mathbf{F}_{\Delta\alpha} + \mathbf{F}_{\Delta T} + \mathbf{F}_R + \mathbf{F}_\eta + \mathbf{F}_G = 0 \tag{1}$$

where the second type of photophoretic force $\mathbf{F}_{\Delta\alpha}$ has a negative z-component $F_{\Delta\alpha,z}$ pointing to the light source,[15] the first type of photophoretic force $\mathbf{F}_{\Delta T}$ and radiation pressure $\mathbf{F}_R$ are along the laser propagation direction, Stokes drag force $\mathbf{F}_\eta$ in air is against the motion direction, $\mathbf{F}_G$ the gravitation force along y direction,[15] as illustrated in Figure 31.

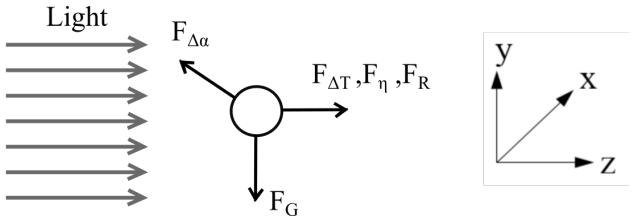

Figure 31: Diagram of optical pulling forces.

The gravitational, scattering, and Stokes' drag forces can be mathematically quantified as,

$$\mathbf{F}_G = \frac{4}{3}\rho g \pi a^3 \tag{2}$$

$$\mathbf{F}_R = \mu(\pi a^2)\frac{I}{c} \tag{3}$$

$$\mathbf{F}_\eta = 6\pi\eta a\mathbf{v} \tag{4}$$

where μ is the absorption coefficient of the particle, a is the Stokes radius of the particle, c is the

speed of light, and η is the medium viscosity, and ρ is the density of the particle. As a result, the pulling speed in z-direction can be estimated by

$$\mathbf{F}_{\Delta\alpha,z} - \mathbf{F}_{\Delta T} - \mathbf{F}_R - \mathbf{F}_\eta = 0 \tag{5}$$

$$v = \frac{\mathbf{F}_{\Delta\alpha,z} - \mathbf{F}_{\Delta T} - \mathbf{F}_R}{6\pi\eta a} \tag{6}$$

From a semi-empirical model,[25,26] the magnitude of photophoretic forces is given by

$$F_{\Delta\alpha} = \frac{I(\pi a^2)}{12c}\frac{\Delta\alpha}{\alpha}\frac{1}{1+(\frac{p}{p_{max}})^2} \tag{7}$$

$$F_{\Delta T} = 2F_{max}\frac{1}{\frac{p}{p_{max}} + \frac{p_{max}}{p}} \tag{8}$$

or $F_{\Delta\alpha} = A(p)I$ and $F_{\Delta T} = B(p)I$, where p is the gas pressure, F_{max} is the maximum $F_{\Delta T}$ force achievable at a pressure p_{max}, which is proportional to laser intensity, and A and B are the pressure-dependent parameters. This gives that $v = \gamma I$, where $\gamma = (A - B - \mu\pi a^2/c)/(6\pi g a)$. This means the pulling speed v of the particle is proportional to the laser intensity I at a given gas pressure.

The semi-empirical model for photophoretic forces assumed a linear light absorption of spherical particles.[25] To explain nonlinear dependence of the pulling speed on laser intensity observed in our experiments, consider the saturation in light absorption by the tiny particle ($\sim 10\mu$m in size) when the laser intensity is strong. Accordingly, both photophoretic forces and scattering force are modified due to absorption saturation as

$$F_{\Delta\alpha} = A\frac{I}{1+\frac{I}{I_{sat}}} \tag{9}$$

$$F_{\Delta T} = B\frac{I}{1+\frac{I}{I_{sat}}} \tag{10}$$

$$F_R = \mu(\pi a^2)\frac{I}{[(1+\frac{I}{I_{sat}})c]} \tag{11}$$

where I_{sat} is the saturation intensity. This leads to the pulling speed as $v = \gamma I/(1+I/I_{sat})$. Figure 22.d shows the theoretical fitting of one of the individual particles in figure 22.a with saturation intensity. Figure 22 shows that as the gas pressure decreases, the saturation intensity decreases. This could be understood as follows: at a lower pressure, there are less gas molecules existing in the chamber and thus less heat is removed from the absorbing particle via the collisions between the gas molecules and the particle. As a result, less laser intensity is required to heat the particle to the absorption saturation state.

It should be noted that the pulled particles move in helical motion. Its trajectory could be approximately described by a linear motion in z-direction and a rotation motion in transverse direction, such that

$$z(t) = z_0 + vt \tag{12}$$

$$x(t) = r_0 cos(\omega t) \tag{13}$$

$$y(t) = r_0 sin(\omega t) \tag{14}$$

where z_0 is the initial axial position, r_0 is the rotation radius, and ω is the rotation angular frequency. For the particle in Fig. 3, $\omega = 2\pi \times 2.5$ kHz and $v = 5.4$ cm/s. As described previously,[15] $\mathbf{F}_{\Delta\alpha}$ force is body-fixed, its longitudinal component $F_{\Delta\alpha,z}$ provides the backward pulling force and one of its transverse components provides the centripetal force F_c for rotation motion, and its tangential component F_t is balanced by the viscous drag force to maintain a stable rotation motion.[15]

The single collimated laser beam can be used to pull many different kinds of absorbing particles over large distances. The chemical compositions of these particles can be characterized with micro-Raman spectroscopy.

4.2 Optical Deflection

From the deflection efficiency data, the particle's trajectory inside the intersection region is related to the laser beam intensity. The motion data indicates that while a particle is inside a particular

region the velocity and rotation are relatively constant. We can consider the motion of a particle in a pulling beam as a translational motion along the negative beam propagation direction, in addition with a rotational motion along the beam axis. Even though a trajectory inside the intersection region is rather complex to describe, a simplified description can be made with the following assumptions:

1. Velocity magnitude remains nearly constant.

2. Rotation frequency remains nearly constant.

3. Velocity direction of translational motion determined by the vector sum of the negative propagation vectors of the pulling and deflection beams, weighting by their intensities at a position after one cycle of rotation.

Suppose a particle enters the intersection region from the middle of the pulling beam with some velocity v_0 and rotation frequency ω_0. The time interval of one rotation cycle is determined as

$$\Delta t = \frac{1}{\omega_0} \tag{15}$$

and the position coordinates of the particle are

$$z_i = z_{i-1} - v_0 \cos(\theta_i)\Delta t \tag{16}$$

$$x_i = x_{i-1} - v_0 \sin(\theta_i)\Delta t \tag{17}$$

where, consistent with previous notation, the z-direction is along the same axis of the pulling beam and the x-direction is along the same axis of the deflection beam and θ is the angle of velocity direction. The new position is the old position plus the distance traveled during the time interval. The minus sign in the equations makes the particle motion the same as seen in the high-speed deflection video. Since the motion is against the laser propagation, the angle θ is determined from the negative of the intensity field vectors at the current position. We can define the intensity vector

of a Gaussian beam given by the equation

$$\mathbf{I}(r) = I_0 e^{-2r^2/w_0^2}\hat{\mathbf{e}} \tag{18}$$

So,

$$\mathbf{I}_{pull}(x,y) = I_{01} e^{-2(x^2+y^2)/w_0^2}\hat{\mathbf{e}}_\mathbf{z} \tag{19}$$

$$\mathbf{I}_{defl}(y,z) = I_{02} e^{-2(x^2+y^2)/w_0^2}\hat{\mathbf{e}}_\mathbf{x} \tag{20}$$

where I_0 is the maximum intensity, r is the location from the beam center, w_0 is the beam waist size or radius, $\hat{\mathbf{e}}_\mathbf{z}$ and $\hat{\mathbf{e}}_\mathbf{x}$ are the unit vectors of the propagation directions of the pulling and deflection beams, respectively. In general, a Gaussian beam is 3D having two spatial coordinates and a propagation direction. However, since most particles have an orbital radius that is around the same size of the particle, only the cross-section of the Gaussian beam need be considered. This reduces the Gaussian beam to one spatial coordinate. Using $w_0 = 0.5$ mm and assigning propagation directions, the intensity vectors of the pulling and deflection beams at $y = 0$ plane are then

$$\mathbf{I}_{pull} = I_{01} e^{-8x^2}\hat{\mathbf{z}} \tag{21}$$

$$\mathbf{I}_{defl} = I_{02} e^{-8z^2}\hat{\mathbf{x}} \tag{22}$$

The intersection region, combined of both beams, is thus,

$$\mathbf{I}_{int} = \mathbf{I}_{pull} + \mathbf{I}_{defl} \tag{23}$$

$$\mathbf{I}_{int} = I_{01} e^{-8x^2}\hat{\mathbf{z}} + I_{02} e^{-8z^2}\hat{\mathbf{x}} \tag{24}$$

The angle at any position can now be calculated as

$$\theta = \tan^{-1}\left(\frac{-\mathbf{I}_{defl}}{-\mathbf{I}_{pull}}\right) \tag{25}$$

$$\theta_i = \tan^{-1}\left(\frac{I_{02}}{I_{01}}\frac{e^{-8z_i^2}}{e^{-8x_i^2}}\right) \tag{26}$$

$$\theta_i = \tan^{-1}\left(\frac{I_{02}}{I_{01}}e^{-8[z_i^2-x_i^2]}\right) \tag{27}$$

The trajectory coordinates were calculated using a Matlab routine. The Matlab routine is provided in Appendix C. Figures 32.c and 32.d respectively show a deflection and passing through trajectory calculated by the routine. Only the deflection beam power was changed to yield the two cases.

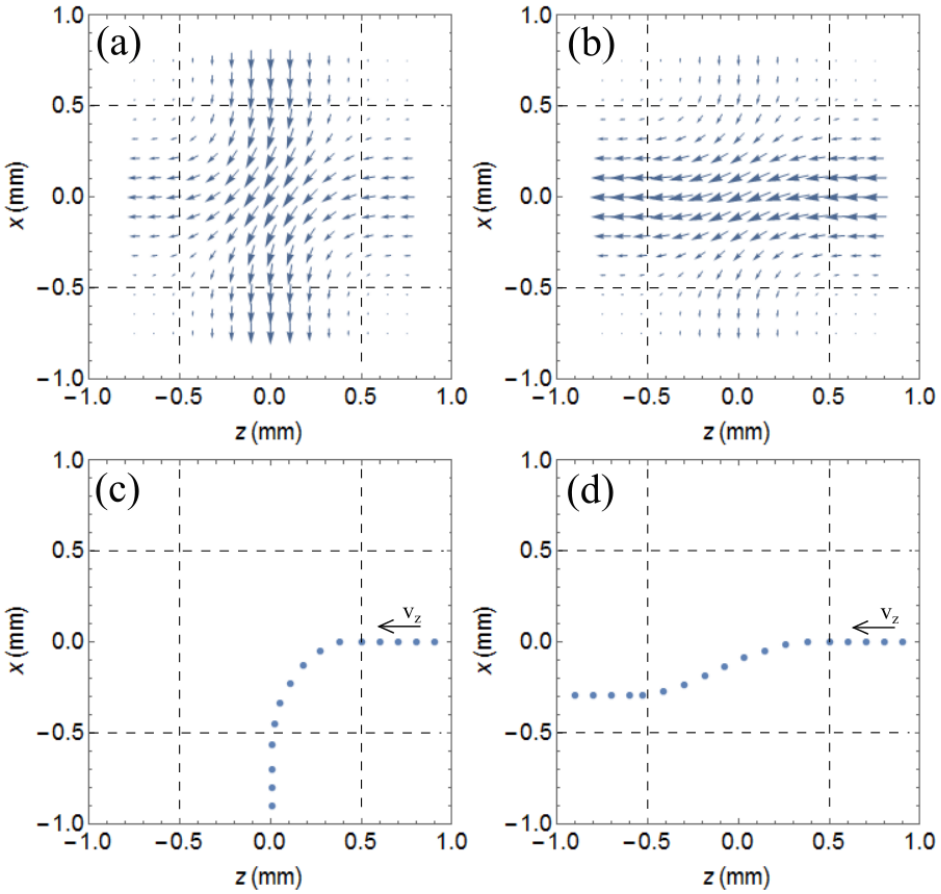

Figure 32: The negative of the laser intensity field is shown for a pulling beam power of 75 mW and deflection beam power of (a) 112.5 mW and (b) 32.5 mW. The beam radius of both beams is $w_0 = 0.5$ mm. The calculated trajectories for a particle with $v_0 = 60$ mm/s and $\omega_0 = 500$ Hz pulled at 75 mW. (c) The particle deflects when the deflection beam is at 112.5 mW. (d) The particle passes through when the deflection beam is at 32.5 mW.

5 Conclusion

As stated in the introduction, the goal of this thesis was the development of optical transportation technology via optical pulling with the application to the characterization of single airborne particles. Shown here in this work is the demonstration for the first time of such technology that accomplishes this goal through the schemes of optical pulling, optical deflection, and optical trapping.

The optical pulling experiment demonstrates the transportation of single airborne particles on meter scale distances for multiple types particles. The optical deflection experiment demonstrates the deflection of optically pulled particles into another transporting pathway. This opens up a method of optically sorting particles. The optical trapping demonstrates the trapping of optically pulled particles. This provides a method of optically selecting particles from the transportation pipeline. It is worthwhile to note the experiments all utilize negative photophoresis force driven by a single Gaussian beam. Negative photophoresis is especially important because the direction of the force is towards the light source, thus particles can be easily captured for analysis. Although the data was only provided for the optical pulling experiment, all experiments can utilize microscopy and Raman spectroscopy techniques for the characterization of bioaerosols and particulate matter in air. Optical manipulation and characterization of single airborne particles are of significance for the analysis related to air pollution, human health, and global climate change.

In addition to the technological development, the optical pulling and optical deflection experiment yielded motion data to further the knowledge of optical manipulation. Both experiments support the motion of transported particles as helical. A saturation limitation is revealed, which consequently may lead to efficient optical transportation technology as well as understanding the limitations of the optical pulling forces. The pulling and deflection models improve the understanding of particle behavior under the effect of negative photophoresis. Complete understanding of photophoretic forces is essential to developing technology which have practical purposes outside of the laboratory setting.

Currently the technology here has been shown useful in pressure environments near 110 Torr

and for high absorbing particles with irregular geometry. The irregular geometry is important because natural particles will have unknown or irregular geometries. However, the pressure environments near 110 Torr limits where the technology can be used. If optical manipulation technology can be utilized at surface level pressures, the technology could be employed as an optical filter for the capture and/or identification of air contaminants. This could be useful for the reduction of smog particulates where smog pollution is prevalent or battlefields where identification of biological agents could prevent deaths. If this technology can be utilized in exosphere pressures, it may be possible to equip a low earth orbiting satellite with this technology to examine particulates in the upper atmosphere. This can be of importance to atmospheric scientists to better understand climate change as well as biologists if biological particles or systems are found to exist there. Future work should be directed toward finding the limitations of this technology.

Experimentally there are plenty of unexplored avenues to consider such as particle, laser beam, or environment properties for future work. Since theoretical models provided for photophoretic forces in the literature[5,25,26] contain quantities from almost every branch of classical physics, there are many factors to consider when trying to determine the optimal or extrema conditions of optical manipulation. Due to the helical motion of an optically pulled particle, there exists a restoring force that must be adapted into trajectory models. This restorative force would vastly improve the deflection model as well as give a limitation for pulled particles in environments with air flow. It is suspected that the restorative force is proportional to the gradient of the laser intensity, however, data is needed to quantify this proportionality. The temperature of an optically manipulated particle is also of interest because photophoretic forces depend on temperature, yet again, data is needed.

In all, optical manipulation of single airborne particles via negative photophoresis has been realized. This is the first time that it has been demonstrated using a single Gaussian beam over meter scale distances. The development of this technology relies on the understanding of photophoretic forces in which there are many avenues of exploration. Even though this technology is still in infancy and emerging, there have been great strides and uses of other optical manipulation technology, namely, the nobel prizes in 1997 and 2001.[7,8] This goes to show the impact of developing

this technology and why investing in future research in this field is still worthwhile.

References

[1] Arthur Ashkin. Acceleration and trapping of particles by radiation pressure. *Physical Review Letters*, 24:156–159, 1970.

[2] Jeff Hecht. Short history of laser development. *Optical Engineering*, 49, 2010.

[3] Vladlen G. Shvedov, Andrei V. Rode, Yana V. Izdebskaya, Anton S. Desyatnikov, Wieslaw Krolikowski, and Yuri S. Kivshar. Giant optical manipulation. *Physical Review Letters*, 105, 2010.

[4] M. Planck. Über das Gesetz der Energieverteilung im Normalspectrum. *Annalen der Physik*, 4:553–563, 1901.

[5] Olga Jovanovic. Photophoresis – light induced motion of particles suspended in gas. *Journal of Quantitative Spectroscopy and Radiative Transfer*, 110:889–901, 2009.

[6] Martin Knudsen. Radiometer pressure and coefficient of accommodation. *Det Kgl. Danske Videnskabernes Selskab. Mathermatisk-fysiske Meddelelser.*, 11:1–75, 1930.

[7] M.H. Anderson, J.R Ensher, M.R. Matthews, C.E. Wieman, and E.A. Cornell. Observation of bose-einstein condensation in a dilute atomic vapor. *Science*, 269:196–201, 1995.

[8] Steven Chu, L. Hollberg, J.E. Bjorkholm, Alex Cable, and A. Ashkin. Three-dimensional viscous confinement and cooling of atoms by resonance radiation pressure. *Physical Review Letters*, 55:48–51, 1985.

[9] C.A. Xie, M.A. Dinno, and Y.Q. Li. Near-infrared raman spectroscopy of single optically trapped biological cells. *Optics Letters*, 27:249–251, 2002.

[10] Peter Vandenabeele. *Practical Raman Spectroscopy: An Introduction*. John Wiley and Sons, Ltd., 2013.

[11] Vladlen G. Shvedov, Anton S. Desyatnikov, Andrei V. Rode, Wieslaw Krolikowski, and Yuri S. Kivshar. Optical guiding of absorbing nanoclusters in air. *Optics Express*, 17, 2009.

[12] K.F. Ratcliff, N.Y. Misconi, and S.J. Paddack. *Solid Particles in the Solar System*. D. Reidel Publishing Co., 1980.

[13] Lin Ling and Yong-qing Li. Measurement of raman spectra of single airborne absorbing particles trapped by a single laser beam. *Optics Letters*, 38:416–418, 2013.

[14] Ze Zhang, Drake Cannan, Jingjiao Liu, Peng Zhang, Demetrios N. Christodoulides, and Zhigang Chen. Observation of trapping and transporting air-borne absorbing particles with a single optical beam. *Optics Express*, 20:16212–16217, 2012.

[15] Jinda Lin and Yong-qing Li. Optical trapping and rotation of airborne absorbing particles with a single focused laser beam. *Applied Physics Letters*, 104, 2014.

[16] Yong-Le Pan, Steven C. Hill, and Mark Coleman. Photophoretic trapping of absorbing particles in air and measurement of their single-particle raman spectra. *Optics Express*, 20:5325–5334, 2012.

[17] Aristide Dogariu, Sergey Sukhov, and Juan Jose Saenz. Optically induced 'negative forces'. *Nature Photonics*, 7:24–27, 2012.

[18] Jun Chen, Jack Ng, Zhifang Lin, and C.T. Chan. Optical pulling force. *Nature Photonics*, 5:531–534, 2011.

[19] Varat Intaraprasonk and Shanhui Fan. Optical pulling force and conveyor belt effect in resonatorwaveguide system. *Optics Letters*, 38:3264–3267, 2013.

[20] David B. Ruffner and David G. Grier. Optical conveyors: A class of active tractor beams. *Physical Review Letters*, 109, 2012.

[21] A. Ashkin, J.M. Dziedzic, J.E. Bjorkholm, and Steven Chu. Observation of a single-beam gradient force optical trap for dielectric particles. *Optics Letters*, 11:288–290, 1986.

[22] O.Brzobohaty, V. Karasek, M. Siler, L. Chvatal, T. Cizmar, and P. Zemanek. Experimental demonstration of optical transport, sorting, and self-arrangement using a 'tractor beam'. *Nature Photonics*, 7:123–127, 2013.

[23] Andrey Novitsky, Cheng-Wei Qiu, and Haifeng Wang. Single gradientless light beam drags particles as tractor beams. *Physical Review Letters*, 107, 2011.

[24] S. Sukhov and A. Dogariu. Negative nonconservative forces: Optical "tractor beams" for arbitrary objects. *Physical Review Letters*, 107, 2011.

[25] Hans Rohatschek. Semi-empirical model of photophoretic forces for the entire range of pressures. *Journal of Aerosol Science*, 26:717–734, 1995.

[26] Gerhard Wurm and Oliver Krauss. Experiments of negative photophoresis and application to the atmosphere. *Atmospheric Environment*, 42:2682–2690, 2008.

[27] M. Kandyla, S. Chatzandroulis, and I. Zergioti. Laser induced forward transfer of conducting polymers. *Opto-Electronics Review*, 18:345–351, 2010.

[28] Lingbo Kong, Pengfei Zhang, Guiwen Wang, Jing Yu, Peter Setlow, and Yong-qing Li. Characterization of bacterial spore germination using phase-contrast and fluorescence microscopy, raman spectroscopy and optical tweezers. *Nature Protocols*, 6:625–639, 2011.

A Experiment Components

Table 2: List of Experiment Components

List of Components	**Specification**
Continuous-Wave Laser	Manufacturer: Coherent Model #: Verdi V-6 Wavelength: 532 nm Beam Diameter: $2.25 \pm 10\%$ mm Beam Divergence: < 0.5 mrad Polarization: $>$ 100:1, vertical, linear Power Stability: $\pm 1\%$
Pulsed Laser	Manufacturer: Continuum Model #: Minilite II Wavelength: 532 nm Beam Diameter: 3 mm Max. Pulse Energy: 25 mJ
Vacuum Parts: (Quantity)	NW25 Aluminum wing clamp: 10 NW25 SS/Viton Centering Ring: 10 NW16 Aluminum wing clamp: 1 NW16 SS/Viton Centering Ring: 1 NW25 $20''$ Metal Hose: 1 NW25 $8''$ Metal Hose: 1 NW25 $4''$ Metal Hose: 1 NW25 Four Way Cross: 1 NW25 Manual Right Angle Valve: 2 NW25 Tee: 1

	NW25 to $\frac{1}{8}''$ Female NPT: 1
Plastic Tube	Manufacturer: McMaster-Carr Part #: 3161T31 Name: Impact-Resistant Polycarbonate $1''$ Square Tube Length: $6'$
Vacuum Pump	Manufacturer: Agilent Technologies Model #: DS 302
Pressure Monitor	Manufacturer: Varian Part #: P101658 Name: 531 Thermocouple Gauge Tube Manufacturer: DigiVac Model #: Model 200 Name: Vacuum Controller
Liquid Crystal Controller Liquid Crystal	Manufacturer: ThorLabs Model #: LCC25 Manufacturer: ThorLabs Model #: LCR-1-VIS Wavelength Range: 450-650 nm Retardence Range: 30 nm - $> \frac{\lambda}{2}$
Mirrors	Manufacturer: Newport Model #: 5101 Name: VIS Dielectric Mirror
Camera	Manufacturer: Casio

	Model #: EX-ZR200
Half-Wave Plate	Manufacturer: ThorLabs Part #: WPH05M-532
X-Y-Z Stage	Manufacturer: ThorLabs Part #: PT3
Optical Pulling	
Polarizing Beam Splitter	Manufacturer: ThorLabs Model #: PBS251
Focusing Lenses f_1 f_2 f_3	Manufacturer: ThorLabs Part #: LB4282 Focal length: 200 mm Diameter: $1''$ Part #: LB4941 Focal length: 100 mm Diameter: $1''$ Part #: LB4915 Focal length: 50 mm Diameter: $\frac{1}{2}''$
Optical Deflection	
Polarizing Beam Splitter PBS_1 PBS_2	Manufacturer: ThorLabs Model #: PBS121 Model #: PBS251
Focusing Lenses f_1, f_3	Manufacturer: ThorLabs Part #: LB4282 Focal length: 200 mm

	Diameter: $1''$
f_2, f_4	Part #: LB4941 Focal length: 100 mm Diameter: $1''$
f_5	Part #: LB4915 Focal length: 50 mm Diameter: $\frac{1}{2}''$
Objective Lens f_6	Manufacturer: Zeiss Working Distance: 12.5 mm Aperture Diameter: $\frac{1}{4}''$
Optical Trapping	
Polarizing Beam Splitter PBS_1 PBS_2	Manufacturer: ThorLabs Model #: PBS121 Model #: PBS251
Focusing Lenses f_1	Manufacturer: ThorLabs Part #: LB4282 Focal length: 200 mm Diameter: $1''$
f_2	Part #: LB4941 Focal length: 100 mm Diameter: $1''$
f_3	Part #: LB4941 Focal length: 50 mm

	Diameter: $1''$
f_4	Part #: LB4915 Focal length: 50 mm Diameter: $\frac{1}{2}''$
Other Equipment	
Power Meter	Manufacturer: Coherent Model #: FieldMax-TOP
Sensor	Part #: 1097901 Name: PM10
Photodiode	Manufacturer: ThorLabs Part #: FDS1010 Size: 10 mm $\times$ 10 mm
Data Acquistion Card	Manufacturer: Measurement Computing Corporation Model #: USB-1208HS-4AO Name: High-Speed DAQ Device
Sample	Manufacturer: Sigma-Aldrich Name: Carbon Size: $<$ 50 nm
	Manufacturer: Thermo Fisher Scientific, Inc. Name: Bermuda Grass Smut Spores Size: $6-8\mu$m
	Manufacturer: Thermo Fisher Scientific, Inc.

	Name: Johnson Grass Smut Spores Size: $6-9\mu$m Manufacturer: Sigma-Aldrich Name: Copper (II) Oxide Item #: 450804 Manufacturer: Central Scientific Name: Iron Filings Item #: 78395B
Neutral Density Filter	Manufacturer: Edmund Optics Inc. Optical Density: 2.5 Transmission: 0.3% Size: 50 mm square
Fluourescent Dye	Manufacturer: Sigma-Aldrich Corp. Name: Rhodamine B λ_{max}: 543 nm

B Matlab Interface

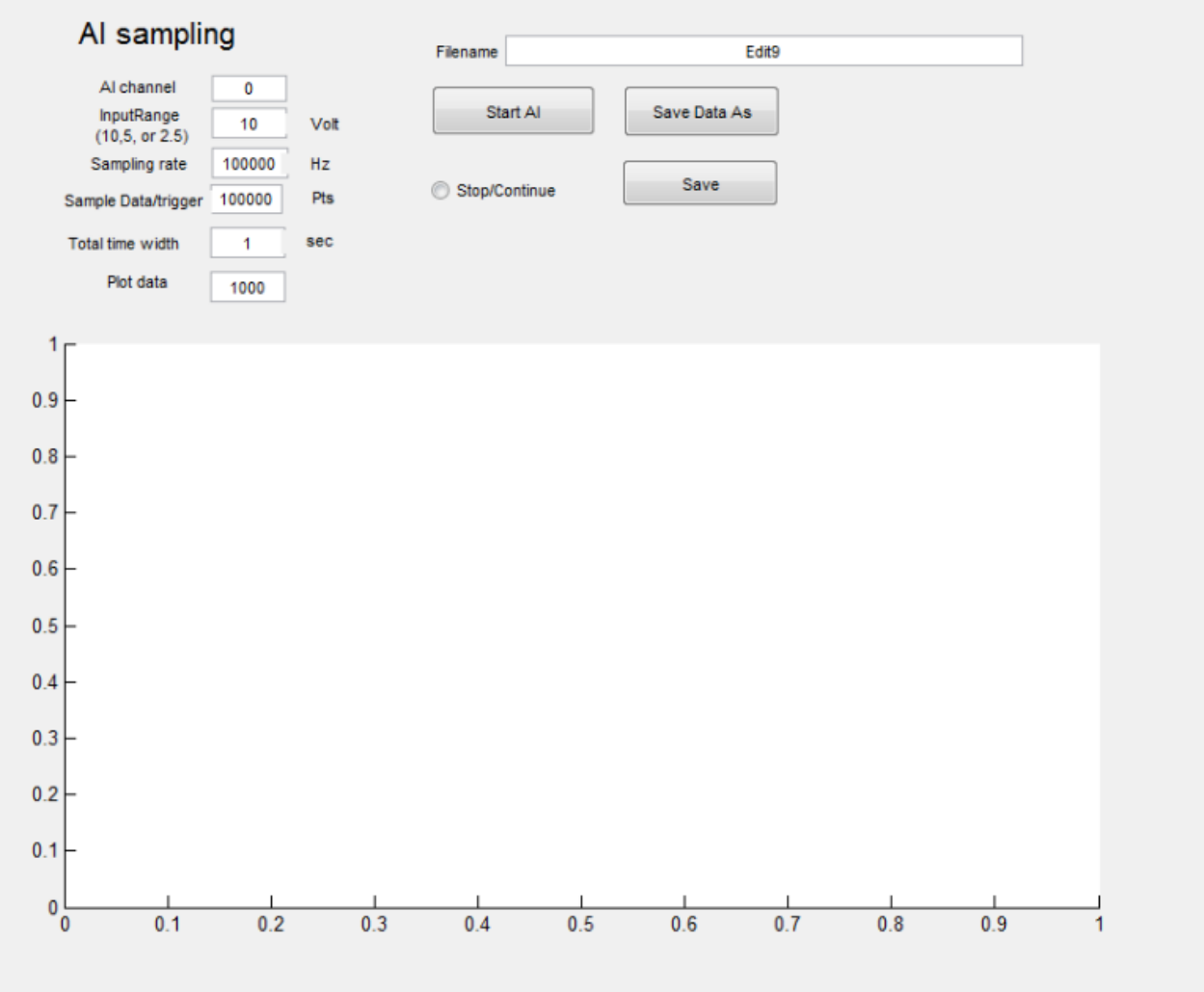

Figure 33: Matlab Interface

The Matlab code interfaces the computer with the DAQ. The code takes advantage of the capability of the DAQ as seen by the input settings of figure 33. A plot is displayed after data acquisition which can help with photodiode position calibration and data quality. The data acquired can be saved in a text file format for further processing in other software.

C Matlab Deflection Trajectory

```
function [x, y] = DeflectionTrajectory(v0,w0,Ip,Id)
%Deflection Trajectory
%This program determines the trajectory of a particle passing through
%intersecting gaussian beams with simple criteria. Assumption
%that v0 and w0 remain constant in the intersection. The new veloctiy
%vector is determined by the intensity field vectors ONLY after one cycle
%of rotation.

%v0 - initial velocity is entered in mm/s
%w0 - initial angular freq. is entered in Hz
%Ip - pulling beam power is entered in mW
%Id - deflecting beam power is entered in mW

%Beam Power in mW. Both beams have same size.
Idefl = Id;
Ipull = Ip;

%Determine the time step
dt = (w0)^-1;

%Setup Placeholder Matrices
i=1;
n=200; %CHEAP TRICK, just a value that overshoots the amount of
       %coordinates generated such that we guarantee the "while" condition
x = zeros(1,n);
y = zeros(1,n);
theta = zeros(1,n);

%Generate the coordinates with our criteria.
```

```
    % 1) stop when particle moves out of intersection
while x(1,i) > -1 && y(1,i) > -.5 ;
    % 2)new coordinates from the previous location
    x(1,i+1) = x(1,i)- v0*dt*cos(theta(1,i));
    y(1,i+1) = y(1,i)- v0*dt*sin(theta(1,i));
    % 3)angle from gaussian intersection
    theta(1,i+1) = atan((Idefl/Ipull)*(exp((-2*(x(1,i+1)+.5)^2)/(.25)))/...
       (exp((-2*(y(1,i+1))^2)/(.25))));
    i = i+1;
end

%Plot Commands
p = linspace(-1,0,10);
q = linspace(-.5,.5,10);
bx0 = 0*ones(1,10);     %beam at x = 0
bx1 = -1*ones(1,10);    %beam at x = .1
by0 = .5*ones(1,10);    %beam at y = .05
by1 = -.5*ones(1,10);   %beam at y = -.05

hold on
plot(x(1,:),y(1,:),'o',bx0,q,'--g',bx1,q,'--g',p,by0,'--g',p,by1,'--g',...
    p,bx0,'--',by1,q,'--')

end
```

D Publication List

Journal Publications

Jinda Lin, Adam G. Hart, and Yong-qing Li. Optical pulling of airborne absorbing particles and smut spores over a meter-scale distance with negative photophoretic force. *Applied Physics Letters*, 106:171906, 2015.

Adam G. Hart, Joshua Mangum and Yong-qing Li. Deflection of optically pulled absorbing airborne particles using negative photophoretic force. (in preparation).

Conference proceedings and presentations

Adam G. Hart, Jinda Lin, and Yong-qing Li. Optical pulling and trapping of airborne absorbing particles and biological smut spores over a meter-scale distance with negative photophoretic force. Poster presentation at Duke University Fitzpatrick Institute for Photonics Annual Symposium, Durham, NC. 2015.